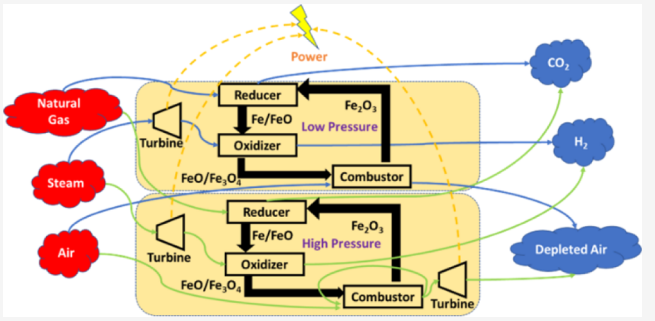
I&EC research
Industrial & Engineering Chemistry Research
pubs.acs.org/IECR
Article

Hydrogen and Electric Power Cogeneration in Novel Redox Chemical Looping Systems: Operational Schemes and Tech-Economic Impact

Qiaochu Zhang, Andrew Tong, and Liang-Shih Fan*

Cite This: *Ind. Eng. Chem. Res.* 2023, 62, 5065−5082
Read Online
ACCESS | Metrics & More | Article Recommendations | Supporting Information

ABSTRACT: Chemical looping water splitting (CLWS) has emerged as a promising technology to produce pure hydrogen with CO_2 capture in a simple and efficient manner. In this study, new schemes for CLWS characterized using integrated turbine-combined CLWS systems (ITC-CLWS) are presented to accomplish cogeneration of hydrogen and electric power. Using natural gas as a feedstock, the ITC-CLWS processes under ambient and pressurized operating conditions are simulated and analyzed based on the desired riser gas velocities that transport solid particles from the combustor to the reducer. The reactors for the ITC-CLWS processes are designed by considering the gas−solid reaction kinetics and multiphase flow properties. The performance results of the ITC-CLWS processes are compared with those of the standard CLWS process and conventional industrial processes including steam methane reforming (SMR) and autothermal reforming of methane (ATR) for hydrogen production. This study reveals that ITC-CLWS can reduce the electricity requirement and enhance process efficiency. Moreover, a novel operating strategy is conceived to yield hydrogen and electric power in a varied proportion in response to their respective fluctuating needs. Based on the economic analyses of the CLWS/ITC-CLWS, ATR, and SMR processes, the levelized cost of hydrogen in the new ITC-CLWS system can be as low as \$1.37/kg (\$ in 2018), which is around 15% lower than those of conventional H_2 production methods with CO_2 capture. Furthermore, an economic sensitivity analysis indicates that the price fluctuations of natural gas and electricity have a significant effect on the H_2 production cost for CLWS/ITC-CLWS.



1. INTRODUCTION

Economical production of hydrogen (H_2) represents presently one of the most exciting industrial focuses because hydrogen is a clean fuel that does not produce CO_2 when utilized, in addition to having a high heating value. The interest in hydrogen production reflects its promising fuel market in the future. Hydrogen is also important for industrial use such as oil refining, metal treatment, and the chemical sector.[1] Thus, processes that can produce hydrogen in a clean, cost-effective, and technologically feasible manner and employ a variety of feedstocks are industrially attractive.

Technologies for H_2 production have a long history of development, which can be dated back to 1800, when English scientists William Nicholson and Anthony Carlisle discovered electrolysis of water. However, despite the simplicity of the process and the ubiquitous raw material, the cost of electrolysis for hydrogen production is estimated to be over \$4/kg, which is still high for current large-scale production.[2] The current methods for the production of hydrogen given in the U.S. Department of Energy's Office of Energy Efficiency and Renewable Energy report have encompassed, in addition to the electrolytic processes, the thermochemical processes, the direct solar water splitting processes, and the biological processes.[3] Presently, the thermochemical processes, including reforming and gasification, represent most of the industrial hydrogen production methods with fossil fuels as the dominant source of industrial hydrogen production.[4,5] Among these methods, natural gas reforming accounts for 76% of the global hydrogen production in 2018.[1] Since the main component of natural gas is methane, natural gas reforming can also be noted as methane reforming. The methane reforming process includes three main steps: syngas [with carbon monoxide (CO) and H_2 as main components] generation, water−gas shift (WGS) reaction, and hydrogen purification.[6] Other steps such as desulfurization and heat recovery may be necessary to maintain the quality of hydrogen produced and the efficiency of the process operation. In this regard, the natural gas containing H_2S can be

Received: October 25, 2022
Revised: February 6, 2023
Accepted: March 6, 2023
Published: March 16, 2023



ACS Publications
© 2023 American Chemical Society

https://doi.org/10.1021/acs.iecr.2c03834
Ind. Eng. Chem. Res. 2023, 62, 5065−5082

Downloaded from pubs.acs.org/iecred/article-pdf/62/12/5065/1101732/ie2c03834.pdf by DOKUZ EYLUL UNIV user on 01 September 2026

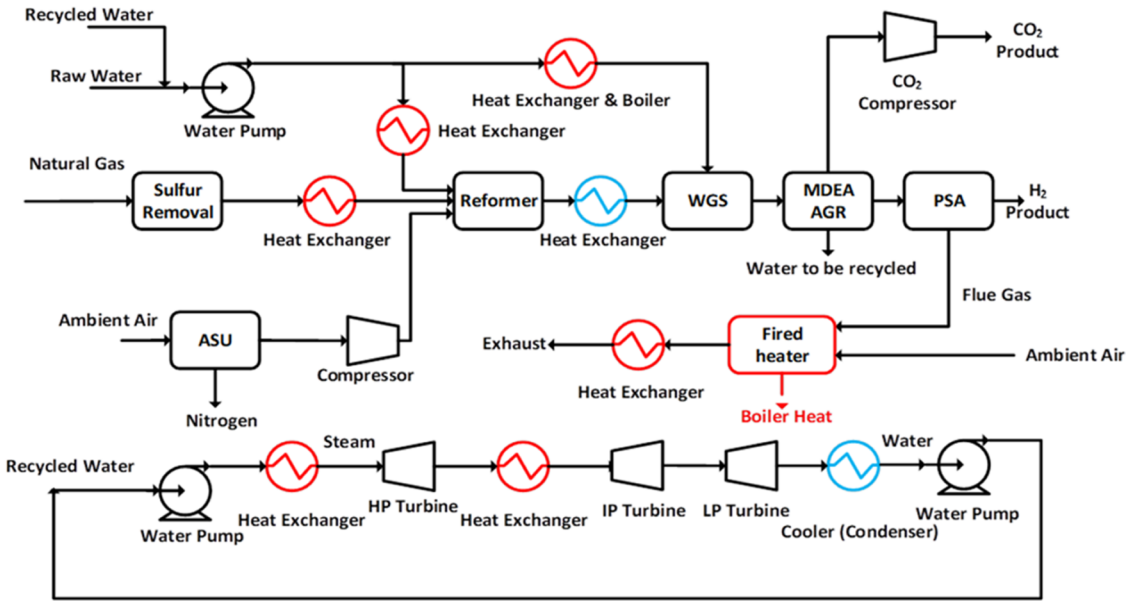


Figure 1. Baseline flow diagram: ATR with CO_2 capture and power generation (red represents heating, and blue represents cooling for heat exchangers).[8,9]

desulfurized through a ZnO bed and then enters a reformer for syngas generation. In the second step, the syngas then goes through the water−gas shift reaction that includes the high-temperature and low-temperature shifts. In the water−gas shift step, the CO is converted to CO_2 through its reaction with steam to produce hydrogen. The last step of the process is pressure swing adsorption (PSA) to separate and purify the hydrogen product from the water−gas shift step. It is to be noted that the modern methane reforming process is to be operated with CO_2 capture in which CO_2 is removed from the syngas after the WGS reaction and the stack gas generation from the boiler/furnace combustion of methane with amine scrubbing. The recycled fuel gas is also combusted to provide the endothermic heat required for the natural gas reforming reaction and steam generation.

There are multiple types of methane reforming approaches in the industry, with the most common two being steam reforming of methane (SMR) and autothermal reforming of methane (ATR). Figure S1 (see the Supporting Information) and Figure 1 show the process diagrams for these two processes.[7−9] In the SMR process, key chemical reactions that take place in different steps of the process are given as follows

Steam reforming of methane reaction[10]

$$CH_4 + H_2O(g) \rightarrow CO + 3H_2,\ \Delta H_{298\,K} = +205\text{kJ/mol} \quad (1)$$

WGS reaction

$$CO + H_2O(g) \rightarrow CO_2 + H_2,\ \Delta H_{298\,K} = -41\text{kJ/mol} \quad (2)$$

Furnace reaction

$$CH_4 + 2O_2 \rightarrow CO_2 + 2H_2O(g),\ \Delta H_{298K} = -803\text{kJ/mol} \quad (3)$$

$$H_2 + \frac{1}{2}O_2 \rightarrow H_2O(g),\ \Delta H_{298\,K} = -242\text{kJ/mol} \quad (4)$$

$$CO + \frac{1}{2}O_2 \rightarrow CO_2,\ \Delta H_{298\,K} = -283\text{kJ/mol} \quad (5)$$

The ATR process for hydrogen production uses natural gas, steam, and oxygen as the feedstock. The major difference between SMR and ATR lies in the reforming reactions. In the SMR reformer, steam is mixed with natural gas for the reforming reaction. Since the steam reforming reaction is endothermic, the reformer is designed to be externally heated through the combustion of natural gas and the recycled fuel gas from PSA. However, in the ATR process, both the steam and pure oxygen from the air separation unit (ASU) are introduced to the autothermal reformer along with natural gas. As the partial oxidation of methane is exothermic, the ATR reformer couples the steam reforming reaction with the partial oxidation reaction to balance the overall heat requirement. Compared to SMR, the ATR process can generate extra combustion heat from the recycled fuel gas from the PSA unit, which can be utilized for power generation through the Rankine cycle.

The ATR reaction in the reformer is given below[11]

$$C_mH_n + \frac{1}{2}mH_2O + \frac{1}{4}mO_2 \rightarrow mCO + \left(\frac{1}{2}m + \frac{1}{2}n\right)H_2,\ \Delta H \approx 0 \quad (6)$$

The SMR method is the most common industrial method utilizing natural gas to produce hydrogen.[12,13] Its operation is established in the existing natural gas pipeline delivery infrastructure. The ATR has also attracted considerable attention for industrial hydrogen production. Both methods can be operated under CO_2-constrained conditions when the current amine technique is applied for the CO_2 capture.

In addition to these two conventional industrial hydrogen production methods described, the chemical looping (CL) technology is an upcoming promising method to produce hydrogen while concurrently capturing CO_2 through unique redox reaction schemes. CL is a versatile technology platform that can be applied for power generation and chemical production including a variety of such operating applications as chemical looping combustion (CLC), chemical looping partial

https://doi.org/10.1021/acs.iecr.2c03834
Ind. Eng. Chem. Res. 2023, 62, 5065−5082

Downloaded from pubs.acs.org/iecred/article-pdf/62/12/5065/1101730/ie2c03834.pdf by DOKUZ EYLUL UNIV user on 01 September 2026

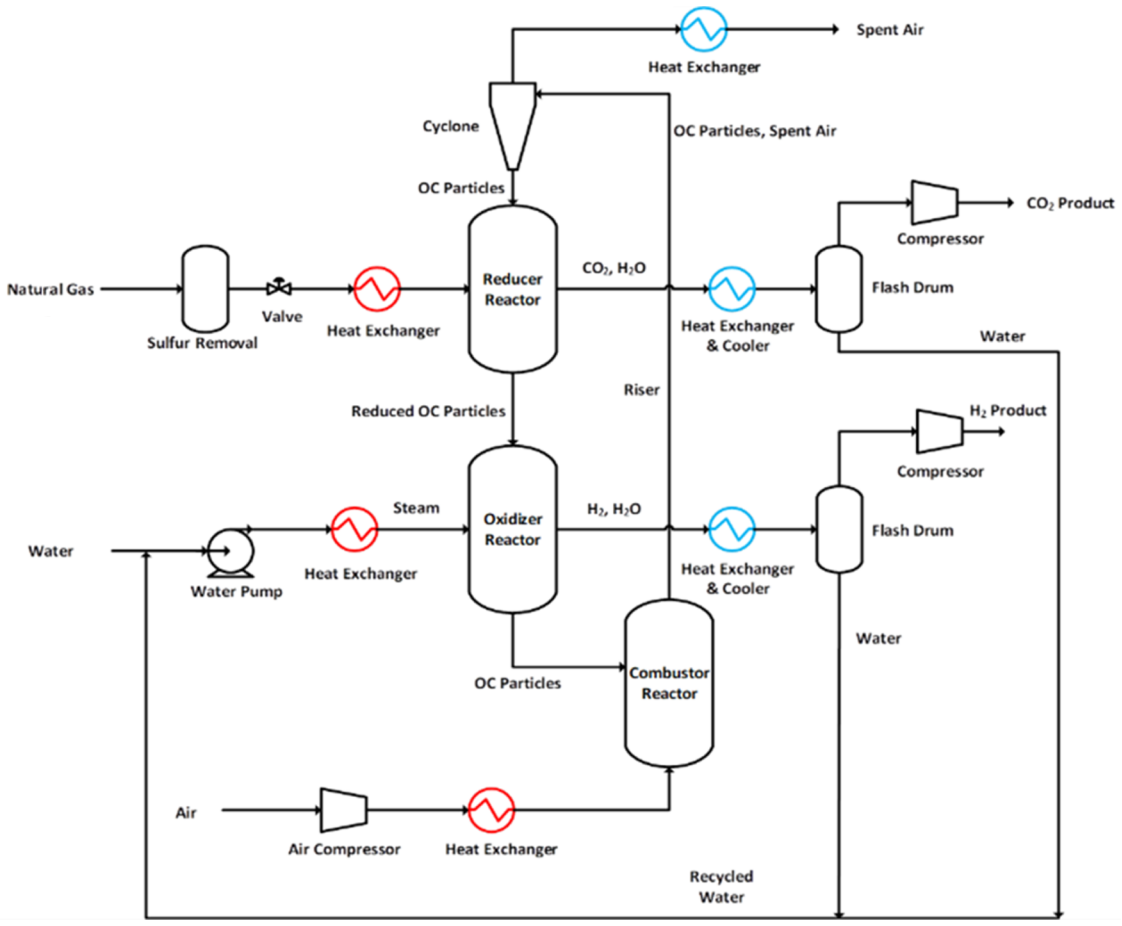


Figure 2. Standard CLWS process (Case 0; red represents heating, and blue represents cooling for heat exchangers).

oxidation (CLPO), and chemical looping water splitting (CLWS).[14,15] The CL technology utilizes the metal oxides as reaction medium to split an overall chemical reaction into two or multiple separate reactions, i.e., reduction and oxidation, which occur in separate reactors. The utilization of metal oxides alters not only the thermodynamic relationship dictating the reaction conditions but also the mode of gas−solid contact in the reactors where the reactions take place, compared to those from the standard processes. As an example, for the CLC process, the CO_2 produced is not mixed with nitrogen from the air so that the CO_2 capture can be conducted with ease. In 2019, Zhang et al. successfully demonstrated a coal-direct CLC 250 kW_{th} pilot plant for power generation and carbon capture.[16] The future upscaling strategies for the CLC commercialization were discussed by Lyngfelt et al.[17] Mei et al. demonstrated in 2021 the feasibility of the oxy-polishing step for the CLC process.[18] Other examples on CLPO to produce syngas can also illustrate the novelty of the chemical looping process. Zhang et al. provided an autothermal operation strategy of the combination of the CLPO and WGS processes for hydrogen production.[19] Liu et al. achieved near-100% CO selectivity in the CLPO with the nanoscaled iron-based particles.[20] Kong et al. explored the dimethyl ether production from coal with CLPO.[21] In contrast to the CLC configuration for power generation and the CLPO configuration for syngas production, the CLWS configuration is designed to directly produce hydrogen. In 2018, Hsieh et al. successfully completed a 250 kW_{th} high-pressure (HP) pilot demonstration of the CLWS system for high-purity H_2 production with CO_2 capture using syngas as the feedstock.[22] Kong et al. used biogas as the feedstock in the CLWS to effectively produce hydrogen through process simulation.[23] He et al. also reported a biomass CLPO coupled with a water/CO_2 splitting process using $NiFe_2O_4$ as the oxygen carrier to produce syngas at a flexible ratio.[24]

Generation of power in addition to hydrogen was studied in several approaches in the literature. Chiesa et al. proposed the recovery and utilization of the excess process heat from the exhaust streams with a combination of gas/steam cycles for power cogeneration.[25] He et al. simulated the H_2 and power cogeneration process with addition of gas turbines at the gas exits of all the reactors in the standard CLWS process.[26] Cormos et al. utilized the combustion of a portion of the hydrogen product from the standard CLWS process in the combined cycle to realize power cogeneration.[27] In contrast to these literature studies, this study first puts forward a cogeneration scheme by integrating the steam turbine with the water feedstock to the CL reactors for power cogeneration. Compared to the conventional Rankine cycle, this new scheme can save the condensation heat of low-pressure (LP) steam in the Rankine cycle for power generation and significantly enhance the process efficiency. Moreover, although some of these literature studies proposed a high energy efficiency of close to 80%, these studies had not appropriately considered the effect of high pressures and their associated gas volumetric flow rate variations on the pneumatic transport of the particles between the reactors. Such an effect that is crucial in quantifying properly the energy efficiency of the process is

https://doi.org/10.1021/acs.iecr.2c03834
Ind. Eng. Chem. Res. 2023, 62, 5065−5082

Downloaded from pubs.acs.org/iecred/article-pdf/62/12/5065/1101730/ie2c03834.pdf by DOKUZ EYLUL UNIV user on 01 September 2026

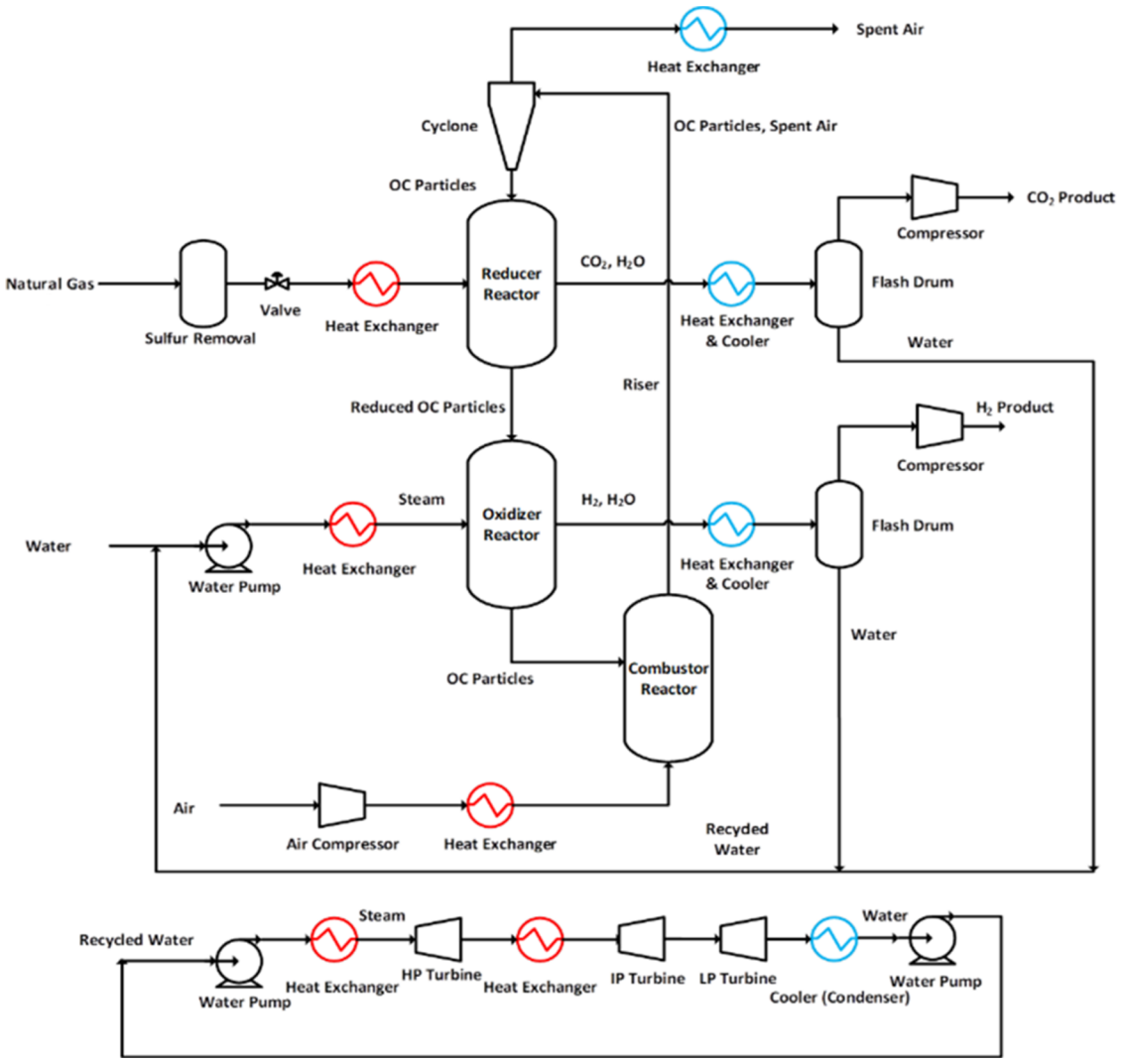


Figure 3. Standard CLWS process combined with the Rankine cycle (Case 1; red represents heating and blue represents cooling for heat exchangers).

thoroughly considered in this study. When the high-pressure effect on the pneumatic transport of the particles between the reactors is considered, the energy efficiency of the process schemes in these literature studies will decrease significantly.

Specifically, in this study, a novel electric power cogeneration strategy is conceived to maximize the thermal efficiency of the CLWS process. Moreover, in contrast to the conventional Rankine cycle for electricity generation, the envisioned new processes integrate steam turbines with the steam generation step for hydrogen production in the CLWS system. In addition to the standard thermodynamic simulation, the velocity requirements for the gas flow to drive the particle circulation and for the gas flow to maintain the particle fluidization in the reactor are considered to improve the CL system design. A novel operation strategy is considered for the cogeneration system to adjust the hydrogen and electricity production rate to meet the market demand. An extensive economic analysis of the new CLWS processes with cogeneration of hydrogen and electricity in comparison to the conventional SMR and ATR processes is also made. The new CLWS process, named as the integrated turbine-combined CLWS (ITC-CLWS) process, is compared in this study with the standard CLWS process and conventional SMR and ATR processes in their system performances to reveal the benefits of the new processes. Finally, the sensitivity analysis of the effects of the variation of multiple cost factors is also conducted for the new CLWS systems. These new cogeneration schemes coupled with their operation under various pressure conditions are revealed to exhibit appreciably higher process efficiency and better economic performance compared to those of the standard CLWS process as well as conventional industrial processes of H_2 production.

2. PROCESS DESCRIPTION

2.1. Standard CLWS Process with and without Electricity Generation (Cases 0 and 1). Figure 2 describes a standard CLWS process under 1 atm, denoted as Case 0, which includes three key operating reactors, namely a reducer, an oxidizer, and a combustor along with a riser, standpipe, and ancillary equipment such as the pumps, the air compressor, and the heat exchangers.[19,22] In the reducer, the natural gas is oxidized to CO_2 and H_2O by the oxygen carrier (OC) particles, made up of hematite (Fe_2O_3) and inert material. Meanwhile, hematite in the OC particles is reduced to a mixture of iron (Fe) and wüstite ($Fe_{0.947}O$). In the oxidizer, the steam is converted into hydrogen by reacting with reduced

https://doi.org/10.1021/acs.iecr.2c03834
Ind. Eng. Chem. Res. 2023, 62, 5065−5082

Downloaded from pubs.acs.org/iecred/article-pdf/62/12/5065/1101730/ie2c03834.pdf by DOKUZ EYLUL UNIV user on 01 September 2026

OC particles, while the reduced OC particles are oxidized to a mixture of magnetite (Fe_3O_4) and wüstite. Finally, preheated air is used to regenerate the mixture back to hematite in a fluidized bed combustor. The regenerated particles then circulate through a riser to the reducer. The CLWS process can be operated under ambient or elevated pressure conditions. The main reactions in the reactors are given below.

Reducer

$$Fe_2O_3 + CH_4 \rightarrow FeO_x + CO_2 + H_2O,\ \Delta H_{298\,K} > 0 \quad (7)$$

Oxidizer

$$FeO_x + H_2O \rightarrow FeO_y + H_2,\ \Delta H_{298\,K} < 0 \quad (8)$$

Combustor

$$FeO_y + O_2 \rightarrow Fe_2O_3,\ \Delta H_{298\,K} < 0 \quad (9)$$

$x < y < 1.33$.

Case 1 combines the standard CLWS process (Case 0) with the Rankine cycle to produce electric power.[25,28] The CLWS section in Case 1 does not vary from the CL process in Case 0, but the excess heat from the CLWS section is provided for the Rankine cycle for electricity generation. Compared with Case 0, the overall thermal efficiency increases with the same amount of hydrogen production and with more electricity generation from the Rankine cycle. The process diagram is shown in Figure 3.

2.1.1. Reducer. The reducer of the CLWS process considered is a counter-current moving bed reactor. The natural gas is conditioned by removal of sulfur and then preheated prior to introducing it to the bottom of the reducer. The OC particles are introduced into the top section of the reducer in a solid−gas counter-current flow pattern to fully oxidize the natural gas, while the OC particles are reduced. Since the exhaust gas stream from the reducer only contains CO_2 and steam, the CO_2 can be readily separated by condensing the steam and removing the water with a flash drum. The separated CO_2 is then pressurized to 152.6 bar for sequestration.[8] Because the reduction reaction of Fe_2O_3 (eq 7) is an endothermic reaction, the temperature decreases throughout the reducer but no lower than 800 °C to maintain the fast kinetics of the reaction. The inlet particle temperature of the reducer is set as 1000 °C.

2.1.2. Oxidizer. The oxidizer of the CLWS process is also a counter-current moving bed reactor for producing hydrogen from water. In this operation, water is first pressurized and heated for steam generation. The hot steam then enters the bottom of the oxidizer and partially oxidizes the reduced OC particles to generate hydrogen. Since the outlet gas from the oxidizer only contains hydrogen and steam (66% H_2 and 34% H_2O in volume fraction), pure hydrogen can be readily obtained by condensing the steam with a flash drum. Finally, the hydrogen product is pressurized to 26.2 bar.[8] Because the reaction in the oxidizer (eq 8) is slightly exothermic, the temperature of OC particles increases as the OC particles flow through the reactor.

2.1.3. Combustor. The OC particles after partial oxidation in the oxidizer flow to the combustor for full oxidation, i.e., full regeneration. The combustor of the CLWS process is operated in a fluidized bed mode with preheated air injected at the bottom of the reactor. The air is compressed or blown into the combustor to oxidize the OC to Fe_2O_3. The OC particles leave from the top of the combustor through a riser to the cyclone on top of the reducer for gas−solid separation. The separated particles enter the reducer, while the exhaust air goes through the heat exchanger and is then released to the atmosphere. The combustor reaction (eq 9) increases the temperature of the particles to 1000 °C and completes the operation loop.

2.2. Integrated Turbine-Combined CLWS Process (ITC-CLWS) for Electricity Cogeneration. In this section, the concept and the scheme of the integrated turbine-combined process are first introduced. The concept is then applied (but not limited) to the new CLWS process with different operating schemes for hydrogen and electricity cogeneration.

Figure 4 shows the process diagram of the classical Rankine cycle in the industry.[29] In this cycle, the raw water is first

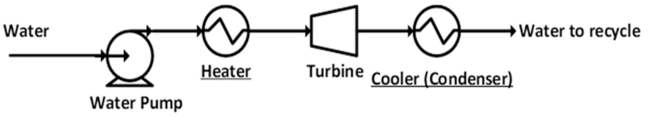


Figure 4. Rankine cycle process diagram.

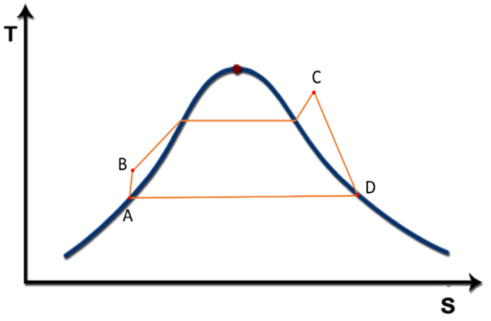


Figure 5. Temperature−entropy diagram of the Rankine cycle.

pressurized through the pump (Figure 5A→B), and the pressurized water is heated for high-pressure steam generation (Figure 5B→C). The high-pressure steam then enters the turbine to produce electricity (Figure 5C→D), after which the cooler condenses the exhaust steam back to water for the next cycle (Figure 5D→A). In industrial processes including the natural gas combined cycle (NGCC), different types of turbines are applied depending on the pressure of the steam, which include the high-pressure (HP) turbine, the intermediate-pressure (IP) turbine, and the low-pressure (LP) turbine.[30] In this study, the HP and IP turbines are applied and integrated with the existing system to enhance the thermal efficiency for electricity generation.

The efficiency of the Rankine cycle is limited by the large amount of heat loss in the condensation of the low-temperature steam in the condenser, which causes the actual thermal efficiency to be less than 60% for typical power stations.[31] However, considering that steam is also widely used in the industry as a feedstock, if the exhaust steam after the turbine can later be utilized in the industrial process as a feedstock, the heat loss from the steam condensation can be avoided, thereby enhancing the thermal energy conversion efficiency significantly. With the combination of steam turbines with the chemical or physical processes that originally require steam as the feedstock, the process can become more energy efficient for electric power generation.

Downloaded from pubs.acs.org/iecred/article-pdf/62/12/5065/1101730/ie2c03834.pdf by DOKUZ EYLUL UNIV user on 01 September 2026

https://doi.org/10.1021/acs.iecr.2c03834
Ind. Eng. Chem. Res. 2023, 62, 5065−5082

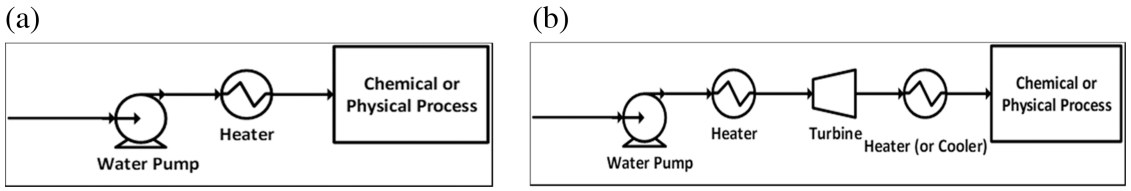


Figure 6. (a) Baseline process diagram with steam utilization. (b) New process diagram integrated with a turbine with power cogeneration.

Conventionally, the Rankine cycle in its operation of electricity generation in a chemical or physical process system is isolated, i.e., not directly linked to the functions of other system components except heat exchange. However, in the new scheme for power generation with the Rankine cycle, mass transfer is also involved in the functions of other system components, forming a tightly integrated operating system. In doing so with this scheme, the efficiency of thermal energy to electricity is increased significantly. Specifically, compared with the conventional scheme of steam utilization (as shown in Figure 6a), the new scheme adds a turbine and heaters before the process unit where the steam from the turbine outlet is utilized as the feedstock (as shown in Figure 6b), with the second heater (or cooler) set under the same conditions of temperature and pressure as those of the original process inlet steam.

There are two sources of water feedstock for the ITC-CLWS process. The first water source is the freshwater makeup after the treatment, and the second is recycled water from the flash drum. The water treatment for the freshwater is assumed to comply with the same standard as the steam cycle requirement in the NGCC process. Based on the simulation results, the recycled water stream only contains H_2O and a trace amount of CO_2. Therefore, both water sources are assumed to satisfy the quality requirement for the proposed open steam cycle system.

It is noted that the heaters in the new scheme can also be replaced with heat exchangers through heat integration of the overall chemical or physical process system. This integrated process requires a water pump to pressurize the water to a pressure higher than that in the original process to satisfy the pressure requirements of the steam turbine, and it can later decrease to a pressure that fits the downstream process unit. In Figure 6b, the first heater between the pump and the turbine is used to vaporize the water and increase the steam temperature to satisfy the requirements of the steam turbine, while the second heater (or cooler) between the turbine and process unit can reheat (or cool) the steam to the temperature that the original process unit requires for the inlet steam. The turbine is placed between the heaters to convert the kinetic energy of steam to electrical energy.

The proposed scheme in the new process can also be illustrated in Figure 7. As shown in the temperature−entropy diagram, A→B→D describes the temperature and entropy change in the original steam utilization process, which consists of two sections: A→B representing the pumping process of water and B→D representing the heating process which converts water to steam for utilization in the baseline scheme. With integration of the steam turbine into the process, the raw water is pumped to a higher pressure, displayed as A→B′ in Figure 7, and heated up for steam generation (B′→C′). The turbine then utilizes the high-pressure steam to generate electric power, and thus, the temperature and pressure of the steam decrease (C′→C). Finally, to ensure the same steam

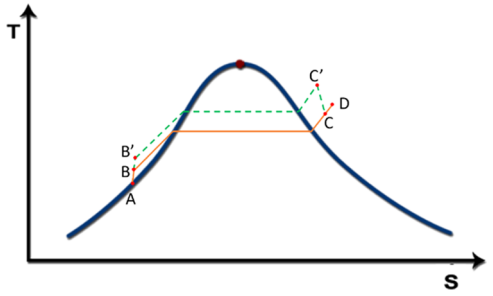


Figure 7. Temperature−entropy diagram of the integrated steam turbine-combined process.

temperature for the inlet of the process unit in the new process, another heater (or cooler) is needed to adjust the temperature to reach the same conditions of the steam as in the original process before the utilization (C→D).

2.2.1. Basic ITC-CLWS Process (Case 2). The integrated turbine-combined technology is applied to the CLWS under 1 atm in case 2 for electricity cogeneration. As shown in Figure 8, water is first pressurized and heated to generate high-temperature and high-pressure steam (566 °C, 166.5 bar), which then enters the HP turbine for power generation. A second heat exchanger heats the steam from the HP turbine (355 °C, 42.8 bar) up to 566 °C before entering the IP turbine. After power generation, the exhaust steam (196 °C, 2.4 bar) goes through another heat exchanger to reach the same designed temperature and pressure (400 °C, 2.4 bar) as it enters the oxidizer in case 0. To maintain the overall heat balance under the autothermal operation mode, the steam input to the oxidizer is less than that in case 0 because a portion of the heat which was used to generate steam in case 0 is utilized to generate electric power instead, so the hydrogen production from the oxidizer decreases. Compared with case 0, the particles at the outlet of the oxidizer in case 2 have a higher ratio of $Fe_{0.947}O/Fe_3O_4$ to generate more heat in the combustor, which is later taken away by a higher air flow rate and then utilized through the heat exchanger for steam generation and preheating.

2.2.2. ITC-CLWS Process with Maximum Hydrogen Production (Case 3). Case 3 is a modified version of case 2 to maintain the same steam injection rate of the oxidizer as case 0 for the maximum hydrogen production as shown in Figure 9. Case 3 has the same hydrogen production as case 0 and produces electricity more than case 1 but less than case 2. The major goal of case 3 is to maximize hydrogen production, considering that case 2 loses some hydrogen production in exchange for more electric power. To generate the same amount of steam as in cases 0 and 1, the steam at the inlet of the oxidizer in case 3 comes from two sources—one from direct heating, while the other goes through the integrated steam turbine-combined process as explained in case 2. The portion of steam from each source can be adjusted so that the

Downloaded from pubs.acs.org/iecred/article-pdf/62/12/5065/1101730/ie2c03834.pdf by DOKUZ EYLUL UNIV user on 01 September 2026

https://doi.org/10.1021/acs.iecr.2c03834
Ind. Eng. Chem. Res. 2023, 62, 5065−5082

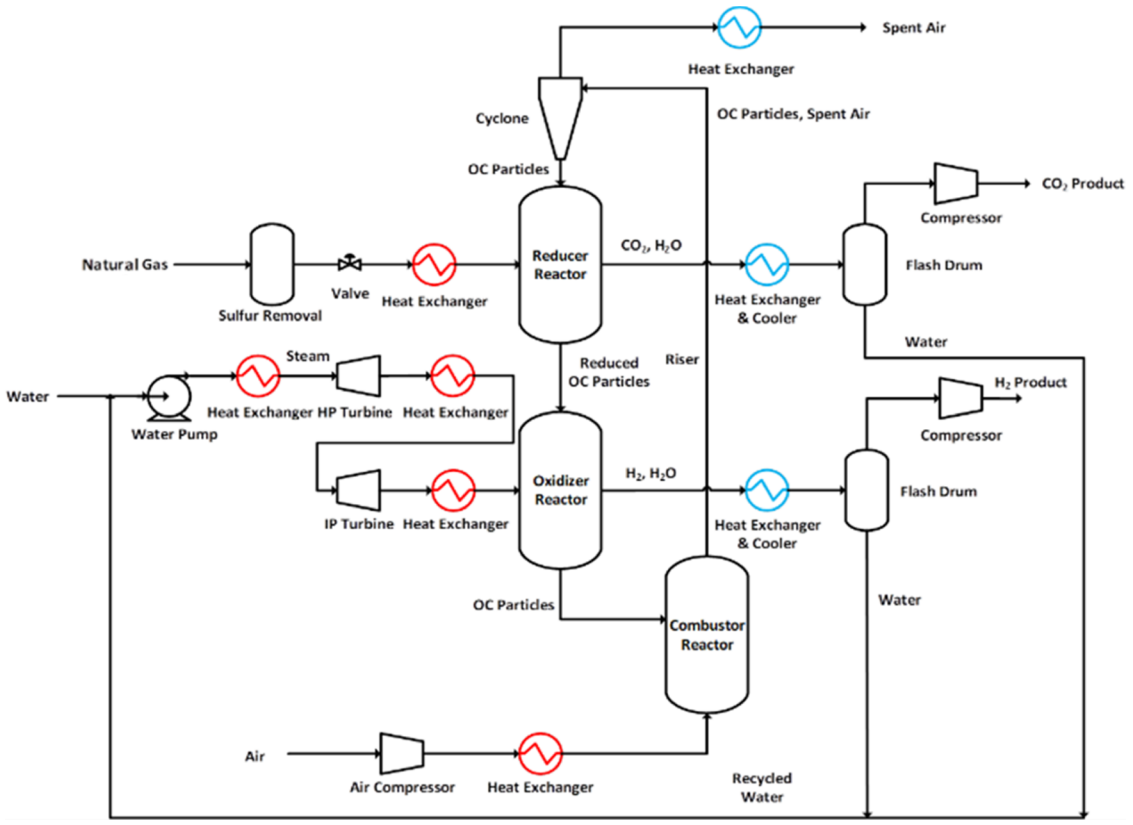


Figure 8. Basic ITC-CLWS process (case 2; red represents heating and blue represents cooling for heat exchangers).

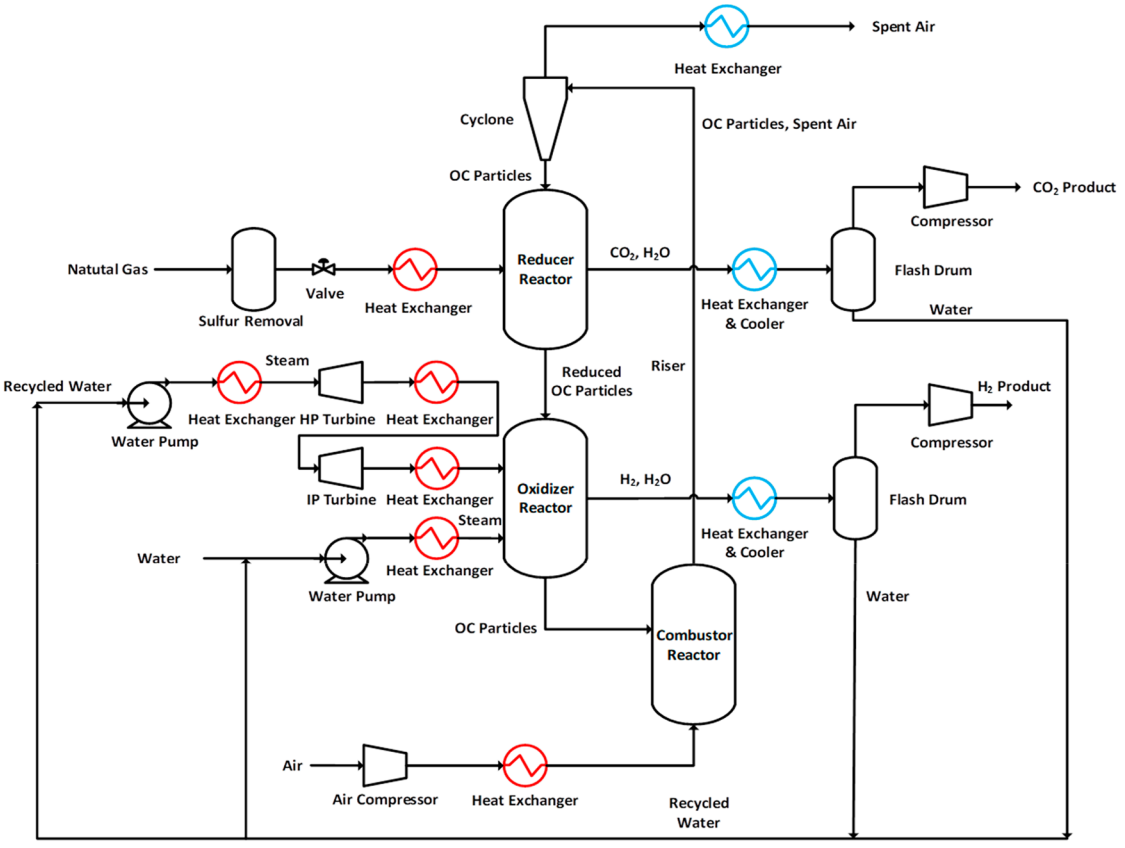


Figure 9. ITC-CLWS process with maximum hydrogen production (Case 3; red represents heating and blue represents cooling for heat exchangers).

Downloaded from pubs.acs.org/iecred/article-pdf/62/12/5065/1101730 2/ie2c03834.pdf by DOKUZ EYLUL UNIV user on 01 September 2026

https://doi.org/10.1021/acs.iecr.2c03834
Ind. Eng. Chem. Res. 2023, 62, 5065−5082

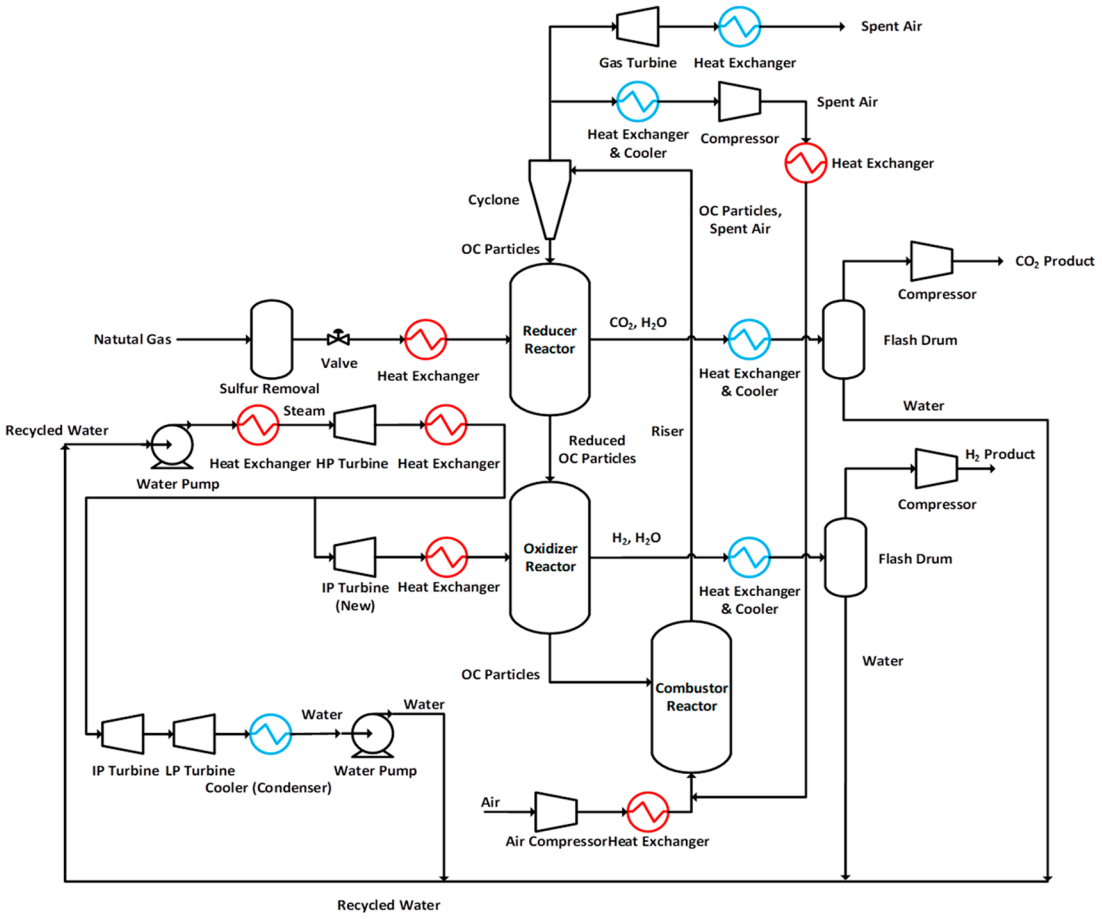


Figure 10. High-pressure ITC-CLWS processes (Cases 4 and 5; red represents heating, and blue represents cooling for heat exchangers).

overall heat balance can be satisfied under the autothermal operation mode.

2.2.3. High-Pressure ITC-CLWS Processes (Case 4: 10 Bar; Case 5: 20 Bar). Compared with the low-pressure operation, the high-pressure ITC-CLWS process produces more electricity but less hydrogen. Higher operating pressures in the reducer and oxidizer decrease the compression duty of the downstream CO_2 and H_2 compressors but require more air to lift the particles up through the riser to the reducer. Since the extra air requires more heat to maintain the same temperature (1000 °C) in the combustor, less steam can be generated for use in the oxidizer under the autothermal operation mode, which results in an increased ratio of $Fe_{0.947}O/Fe_3O_4$ for the OC particles at the oxidizer outlet, leading to a higher rate of heat generation in the combustor. Meanwhile, to reduce the compression energy in the air compressor, a portion of the combustor exhaust gas (case 4: 60%; case 5: 70%) is cooled with heat recovery, recompressed, and recycled to the combustor, while the remaining combustor exhaust gas is sent to a gas turbine for power generation and heat exchangers for heat recovery before being released as shown in Figure 10. On steam utilization, all the water is first pumped to 168 bar before being heated to generate steam. All the steam generated then passes through the HP turbine for power generation. A portion of the exit steam (case 4: 46%; case 5: 74%) from the HP turbine goes through the Rankine cycle to generate electricity. The remaining exit steam then enters an IP turbine, different from that used in the Rankine cycle, and the heat exchanger, to reach a desired steam temperature (400 °C) for its injection to the oxidizer.

3. METHODOLOGY

In this section, a detailed account of the model setup for evaluating the performance of cases 0−5 and ATR given in Section 4 is provided. The model setup considers operating parameters, reactor design, and Aspen thermodynamic simulation. The production cost structure and assumptions as well as the rules for the equipment cost calculation are also presented in this section.

3.1. Operating Parameter Setup. Optimal operating parameters are explored and configured for the CLWS/ITC-CLWS processes as given below, including the particle circulation rate, the air injection rate, and the steam injection rate.

3.1.1. OC Particle Circulation Flow Rate. The particle circulation rate is one of the most important parameters that have a significant effect on the design of the CLWS/ITC-CLWS system. It is determined by the reducer operation specifications. To fully oxidize the reducing gas to H_2O and CO_2 through the reducer for the ease of downstream CO_2 separation and subsequent CO_2 compression, the particle flow rate is specified based on the minimum Fe_2O_3 flow rate to fully oxidize the natural gas. Detailed discussion on the relationship of the particle circulation flow rate, the reducing gas flow rate, and reaction thermodynamics is available in earlier publications.[32]

https://doi.org/10.1021/acs.iecr.2c03834
Ind. Eng. Chem. Res. 2023, 62, 5065−5082

Downloaded from pubs.acs.org/iecred/article-pdf/62/12/5065/1101730/ie2c03834.pdf by DOKUZ EYLUL UNIV user on 01 September 2026

3.1.2. Air Injection Rate. Air is utilized in the combustor to fully oxidize the $Fe_{0.947}O/Fe_3O_4$ in the OC particles to Fe_2O_3 and heat particles to 1000 °C for the reducer operation. To accomplish fast reactions in the combustor, the minimum oxygen concentration of the combustor exhaust gas is given as 3%, compared to the 2% in the baseline combustion.[8] In addition to performing the reaction function, the exhaust air also serves as transport medium that lifts the particles from the combustor through the riser to the reducer. It is noted that under the operation of low pressure at less than 3 bar, the air flow required to maintain the minimum oxygen concentration in the combustor exhaust gas is adequate to lift the particles in the riser. However, for the high-pressure CLWS/ITC-CLWS system operation over 5 bar, the gas volume reduction effect due to an increase in pressures is such that the air flow required to maintain the minimum oxygen concentration in the combustor exhaust gas is not adequate to lift the particles in the riser. Thus, under the high-pressure conditions, the required air flow rate in the combustor needs to be higher, considering both the riser gas flow requirements and the minimum oxygen concentration (3%) constraint in the combustor exhaust gas.

3.1.3. Steam Injection Rate. As the steam injection flow rate to the oxidizer is highly related to the hydrogen production rate in the counter-current moving bed oxidizer, the H_2 yield can be evaluated, considering the thermodynamic limits of the H_2O and $Fe/Fe_{0.947}O$ reaction (eq 8). The hydrogen production increases with an increase in the steam injection until the reduced iron oxide is oxidized to Fe_3O_4. However, instead of converting all the $Fe/Fe_{0.947}O$ species to Fe_3O_4 in the oxidizer, consideration is made with respect to the steam oxidization of the reduced OC to a mixture of $Fe_{0.947}O/Fe_3O_4$, so as to allow sufficient heat to be generated in the combustor (eq 9) to bring up the particle temperature to 1000 °C for the system autothermal operation.

3.2. CL Reactor and Flash Drum Design Specifications. The proper design of the CL reactors and the ancillary equipment (flash drum) is necessary to ascertain feasible operating conditions such as pressure and temperature in the reactors as well as the capital cost calculation. Furthermore, the design of the CLWS/ITC-CLWS reactor assembly system includes two moving bed reactors (reducer, oxidizer) and one fluidized bed reactor (combustor), along with the riser gas requirement that is strongly associated with the particle circulation rate conditions. The flash drums intended for the separation of water and H_2 or CO_2 in the CLWS/ITC-CLWS cases are designed in this study. Data required for reactor and flash drum designs and gas and particle properties are obtained from the Aspen simulation. Furthermore, the pressure drops in the reactors, which is calculated based on the design applied to the simulation. In this study, the OC particle in the calculation is assumed to be spherical with a diameter of 1.5 mm and a density of 3300 kg/m^3. The geometrical shapes of these CL reactors are assumed to be a cylinder with the ratio of H/D specified between 0.6 and 3. All the parameters in the equations used are in the international units (IU).

3.2.1. CLWS/ITC-CLWS Moving Bed Reactor (Reducer and Oxidizer) Design Specification. To quantify the dimensions of the moving bed reactors, the superficial gas velocity at minimum fluidization (MFV) is first calculated based on the gas and particle properties at the reactor outlet, obtained from the simulation results, using the equation of Wen and Yu.[33] The actual superficial gas velocity of the moving bed reducer is designed as 80% of the MFV.[22]

Wen and Yu's equation given below is used to calculate the MFV.

$$Re_{pmf} = \sqrt{33.7^2 + 0.0408Ar} - 33.7 \tag{10}$$

$$Re_{pmf} = \frac{\rho U_{mf} d_p}{\mu} \tag{11}$$

$$Ar = \frac{\rho(\rho_p - \rho) g d_p^3}{\mu^2} \tag{12}$$

where Re_{pmf} is the particle Reynolds number at minimum fluidization, Ar is the Archimedes number, ρ is the gas density, ρ_p is the particle density, U_{mf} is the superficial gas velocity at minimum fluidization, d_p is the particle diameter, g is the gravitational acceleration, and μ is the gas viscosity.

The height of the reactor is determined from the gas and solid residence time, whichever yields a larger reactor volume. The minimum gas residence time for the CLWS/ITC-CLWS reactors under 1 atm is set as 2 s with particle residence time set as 30 min.[22] Based on Mendiara et al.'s experimental study of reaction kinetics, the reaction order is close to 1 for the Fe_2O_3 reaction with CH_4, CO, and H_2.[34] The apparent reaction order is also equal to 1 for the first-order reaction with internal diffusion control with a large value of Thiele modulus.[35] In this study, the apparent reaction order of 1 for OC reacting with gases is applied to estimate the required reactor residence time under different operating pressures. For a high-pressure moving bed reactor, the minimum residence time required for the OC particles is shortened through an inverse scaling relationship with the pressure (3 min for case 4 and 1.5 min for case 5) due to an increased reaction rate with pressures, while the required gas residence time remains unchanged due to the counteracting pressure effects on reaction rates and gas volume flow rates.

3.2.2. CL Fluidized Bed Reactor (Combustor) Design Specification. The MFV for the combustor is also calculated using the same method as the reducer based on Wen and Yu's equations (eq 10). The designed superficial gas velocity is specified as three times the MFV. The cross-sectional area is calculated using the combustor gas volume flow rate divided by the superficial gas velocity. Considering the well-mixed property of the fluidized bed reactor, the minimum particle residence time for the combustor is set as 15 min at 1 atm with a minimum gas residence time of 2 s. Assuming that the apparent reaction order is close to 1, the designed minimum solid residence time is shortened to 1.5 min for both 10 bar and 20 bar cases with the designed minimum gas residence time unchanged. The bed expansion is calculated using the equation by Cai et al.[36]

$$\frac{H_f}{H_{mf}} = 1 + \frac{21.4 \times (U - U_{mf}^*)^{0.738} d_p^{1.006} \rho_p^{0.376}}{(U_{mf}^*)^{0.937} \left(\frac{M_g p}{p_a}\right)^{0.126}} \tag{13}$$

where H_f is the fluidized bed height, H_{mf} is the bed height at minimum fluidization, U is the gas superficial velocity, U_{mf}^* is the minimum fluidization velocity at ambient temperature, M_g is the molecular weight of gas, p is the total pressure, and p_a is the ambient pressure. The bed voidage derived from the bed

Downloaded from pubs.acs.org/iecred/article-pdf/62/12/5065/1101730/ie2c03834.pdf by DOKUZ EYLUL UNIV user on 01 September 2026

https://doi.org/10.1021/acs.iecr.2c03834
Ind. Eng. Chem. Res. 2023, 62, 5065−5082

expansion is then used to determine the height of the fluidized bed reactor.

3.2.3. Riser Gas Requirement. The riser is placed on top of the combustor to pneumatically transport the particles to the cyclone above the reducer. In the riser, the solid volume fraction is estimated as 1% and the minimum superficial velocity of the particles is designed as 4 m/s. The required gas flow velocity is determined by balancing the gravity and the drag force on the particles. The relationship between the drag coefficient and the Reynolds number is given below.[37]

$$C_D = \frac{18.5}{\mathrm{Re}^{0.6}},\ 2 < Re_t < 500$$

$$C_D = 0.44,\ 500 < Re_t < 2 \times 10^5 \quad (14)$$

where C_D is the drag coefficient and Re_t is the Reynolds number at the terminal velocity.

3.2.4. Flash Drum Design. In this study, the flash drum is designed in the shape of a cylinder for separation of water from H_2 or CO_2 product at 35 °C. The Souders−Brown equation given below is applied for determining the maximum vapor velocity in the vapor−liquid separation vessel.[38]

$$v = k\sqrt{\frac{\rho_L - \rho_V}{\rho_V}} \quad (15)$$

where k is a constant for a given pressure and drum structure; ρ_L is the liquid density; and ρ_V is the vapor density. The H/D ratio of the flash drum is specified between 1.5 and 3. The liquid level is set as 0.5 of the total drum height with the residence time of the condensed liquid designed as 5 min.

3.3. Aspen Model Setup and Process Analysis Assumption. In this study, cases 0−5 and ATR are simulated using ASPEN Plus V11 software. The preheating temperatures of steam, air, and natural gas before entering the reactors are set as 400 °C. The outlet stream temperature from the hot side of the heat exchanger is designed to be 120 °C after heat recovery, and the minimum temperature difference during the heat transfer is maintained above 10 °C using the zone analysis function in Apsen MHeatX block. The overall system is operated under the autothermal (without outside heat sources) operation conditions. The OC particle composition is set as 30% Fe_2O_3 and 70% SiC based on a former study.[39] The thermodynamic properties and the list of species used in the process simulation are shown in Table S1 (see the Supporting Information), and the natural gas composition is listed in Table S2 (see the Supporting Information). The simulation of H_2S removal is not considered in this study, so the natural gas injected into the reducer is assumed to be sulfur-free.

The simulation strategy of the CLWS process in Aspen has been demonstrated in previous studies.[32,39] The reducer and oxidizer are simulated using a series of five RGibbs reactor models, while the combustor is simulated with one RGibbs block. This modeling method has also been verified using the experimental data in previous publications.[14,15,40]

3.4. Simulation Setup. In the Aspen simulation, the CO_2 and H_2 products are compressed to 152.6 and 26.2 bar, respectively.[8] The compressor is configured with an isentropic efficiency of 80% and a mechanical efficiency of 95%. The multistage compressor is designed with an equal compression ratio of less than 3 and an interstage cooling temperature of 35 °C. The setup of the turbine system is based on the specifications of the turbine system described in the National Energy Technology Laboratory (NETL) baseline report.[41] The amine scrubber, i.e., the MDEA CO_2 removal unit, as well as the PSA unit in the ATR processes is simulated with an Aspen Sep block using the yield from the baseline report.[8] Unlike the CL technology that has in situ CO_2 separation, the conventional CO_2 removal process like the amine scrubber requires additional heat for the steam reboiler to regenerate the MDEA solution. The MDEA unit specified in this study requires a regeneration heat of 3.7 MJ per kg of CO_2 separated.[8] The PSA unit is designed to have an H_2 recovery rate of 80%, with the rest of the fuel gas combusted to support steam generation.[8]

In the ATR simulation, an RGibbs block is applied to simulate the autothermal reformer, and the 2-stage WGS process (high-temperature WGS and low-temperature WGS) is simulated with two adiabatic REquil models in Aspen, where the WGS reaction (eq 2) reaches the thermodynamic equilibrium. The inlet temperatures of REquil blocks are set at 345 °C and 204 °C. In addition, other design specifications for this study are listed in Table S3 (see the Supporting Information).

3.5. System Evaluation Parameters. For comparing the performance of the CLWS/ITC-CLWS cases, SMR, and ATR, three system parameters that reflect the energy conversion from natural gas to hydrogen or both hydrogen and electric power are introduced.

3.5.1. H_2 Yield. The H_2 yield indicates the amount of hydrogen produced per mole of natural gas, defined in eq 16.

$$H_2\ \text{yield} = \frac{H_2\ \text{molar flow in the product}}{\text{natural gas molar flow in the feedstock}} \quad (16)$$

A higher H_2 yield means that the natural gas is used more efficiently for H_2 production.

3.5.2. Cold Gas Efficiency (CGE). The CGE measures the energy conversion from the feedstock to products in terms of the lower heating value (LHV). The CGE is defined as the LHV of H_2 divided by the LHV of natural gas, as given in eq 17.

$$\mathrm{CGE} = \frac{\mathrm{LHV\ of\ H_2}}{\mathrm{LHV\ of\ natural\ gas}} \quad (17)$$

With this definition, the CGE is proportional to the H_2 yield. This is an important parameter to reflect on the energy efficiency of the feedstock to H_2.

3.5.3. Effective Thermal Efficiency (ETE). Compared with the CGE, the ETE is a more accurate way to evaluate the energy conversion efficiency, as it considers not only the LHV of the fuel and the product but also the power consumption or generation in the process. The ETE is defined as the sum of the LHV of H_2 and power generation divided by the LHV of the feedstock, as given in eq 18 [8]

$$\mathrm{ETE} = \frac{H_2\ \text{product LHV} + \text{power generation}}{\text{LHV of natural gas}} \quad (18)$$

Based on the formula, the higher the ETE is, the more efficient the process will be.

3.6. Economic Assessments. The economic analysis was conducted to compare the levelized cost of hydrogen (LCOH) for cases 0−5, SMR, and ATR at the same natural gas feed rates. The LCOH is defined as the price at which the generated hydrogen should be sold for the system to break even at the end of its lifetime, according to eq 19.[42] The LCOH is a

Downloaded from pubs.acs.org/iecred/article-pdf/62/12/5065/1101732/ie2c03834.pdf by DOKUZ EYLUL UNIV user on 01 September 2026

https://doi.org/10.1021/acs.iecr.2c03834
Ind. Eng. Chem. Res. 2023, 62, 5065−5082

measure of the average net present cost of hydrogen production, which includes capital costs, operation and maintenance (O&M) costs, and fuel costs over the plant's life. All the cost, price, and income of this study are given in base-year (2018) $.

$$\mathrm{LCOH} = \frac{\sum_{t=0}^{n} (I_t + O_t + T_t + F_t)/(1 + r)^t}{\sum_{t=0}^{n} H_t/(1 + r)^t} \quad (19)$$

where n is the number of years since 2018 (n = 30 + 3 in this study), I_t is the Investment in the tth year, O_t is the O&M cost in the tth year, T_t is the tax cost in the tth year, F_t is the interest cost in the tth year, H_t is the hydrogen production in the tth year, and r is the after-tax weighted average cost of capital (ATWACC), which is specified as 8.13% in this study (Table 1).[43]

Table 1. Important Economic Parameters and Assumptions in the Analysis[43,44]

parameters	value
debt percent	45%
starting year of construction	2018
construction period (in year)	3
plant economic life (in year)	30
ATWACC	8.13%
cost escalation (electricity, O&M, fuel, etc.)	3.0%
income tax rate	38%
effective capacity factor (CF)	90%
solid attrition rate	0.0114%
1-year total hours	8760
loan period (in year)	15
interest rate on debt	5.50%
capital cost escalation	3.60%
electricity loss during transmission for selling	5%

It is assumed that the construction of the plant starts in 2018 and will last for 3 years with a plant life of 30 years.[44] During the 3-year construction period, 10, 60, and 30% values of TOC are invested in view of the recommendations provided in the NETL report.[44] In this study, the solid attrition rate per hour defined as the weight percentage of solid particles that are worn to become powder during the circulation each hour is assumed to be 0.0114%. This assumption is based on the jet-cup studies of the experimental particles tested. The electricity loss during the transmission to customers is estimated as 5% of the total net electric power. Cost escalation, interest, and tax during the construction and operating periods are also considered as per the recommended rates given in the NETL guideline report.[44] The debt percentage is set as 45% for this plant, as it is assumed that the plant is a high-risk investor-owned utility with a loan period of 15 years using an equal loan payment method.[44] The after-tax weighted cost of capital is defined as the annual discount rate for both debt and equity after eliminating tax from the income.[43] These important parameters discussed above for economic assessment are given in Table 1.

The method to estimate the hydrogen production cost (Table S4, see the Supporting Information) is, to a considerable extent, based on the U.S. National Energy Technology Laboratory (NETL) guideline reports. In this study, the overall capital investment at the starting period, also known as the total overnight cost (TOC), consists of the total plant cost (TPC), preproduction costs (PC), inventory capital costs (ICC), initial costs for catalyst and chemicals (ICCC), land costs, other owner's costs (OOC), and financing costs (FC). The TPC estimates include the bare erected costs (BEC) for the equipment, engineering, construction management, home office, and fees (Eng'g CM, H.O., and fee) and contingency values. The detailed structure to estimate the TOC is given in Table S4 (see the Supporting Information) by summing up the TPC, PC, ICC, ICCC, land costs, OOC, and FC. The fuel cost is estimated by the overall natural gas cost with the average annual capacity factor set as 90%. The O&M costs can be divided into fixed O&M costs and variable O&M costs. The fixed O&M costs include operating labor costs, maintenance labor costs, administration and support costs, property taxes, and insurance costs, while the variable O&M costs include maintenance material costs, chemical costs, electricity costs, solid waste disposal costs, and carbon dioxide emission tax costs. To calculate the BEC of chemical plants, the cost of each equipment component is estimated separately. The capacity (S) of the equipment is connected to the equipment cost (C) through eq 20, with the assumption that the number of equipment components remains unchanged between the reference and this study. The component cost (C) is calculated by scaling the capacity with the factor (n) from the reference equipment price. The reference equipment prices from the NETL baseline reports for NGCC, methanol production, and H_2 production used in this study are given in Table S5 (see the Supporting Information).[8,9,41] The chemical engineering plant cost index (CEPCI) is applied to relate the costs of process equipment in the reference year to those in the base year (2018 in this study).[45,46]

$$C = C_0\left(\frac{S}{S_0}\right)^n \cdot \left(\frac{\mathrm{CEPCI}_{2018}}{\mathrm{CEPCI}_x}\right) \quad (20)$$

where C is the estimated cost of the equipment, S is the required capacity for the equipment, and S_0 is the equipment capacity for the reference equipment.

The overall CL reactor system cost includes the costs of reactors, which are estimated as half of the CL reactor system cost and accessory equipment such as cyclone and high-temperature piping.[47] The capital costs of the CL reactors in this study are calculated by scaling the volume of the steel material required for the CLC reactors in the NETL report.[47] For the pressurized CL reactor sizing, rules in Section UG-27 of the American Society of Mechanical Engineers (ASME) standard are applied to calculate the thickness of the pressure vessel.[48] In addition, the flash drum cost is estimated based on the formula in Douglas's book for pressure vessels as given below.[49]

$$\$ = \left(\frac{M\&S}{280}\right)101.9D^{1.066}H^{0.802}(2.18 + F_c) \quad (21)$$

where $M\&S$ is the Marshall and Swift cost index (1038.2 in 2018), D is the diameter, H is the height, and F_c is the correction factor. Except for the CL reactor system and flash drum, the costs of other equipment are directly scaled by eq 20 with reference to Table S5 (see the Supporting Information).

In addition to the capital cost, the fixed O&M costs are calculated based on the production cost structure given in Table S4 (see the Supporting Information), while the variable O&M costs are estimated with reasonable assumptions about the prices of chemicals, services, and fuel as given in Table S6

Downloaded from pubs.acs.org/iecred/article-pdf/62/12/5065/1101730/ie2c03834.pdf by DOKUZ EYLUL UNIV user on 01 September 2026

https://doi.org/10.1021/acs.iecr.2c03834
Ind. Eng. Chem. Res. 2023, 62, 5065−5082

(see the Supporting Information). Based on the U.S. Energy Information Administration (EIA) report given in 2018, the base electricity price in the economic analysis is set as $69.2 per MWh[50] and the natural gas base price is set as $191 per ton.[51] The CL particle price is set as $4000 per ton based on the expense estimation of the OSU CL particles. The cost of CO_2 transport and storage is set as $10/ton CO_2.[52] Other material or service prices such as those of MDEA solutions and solid waste disposal are listed in Table S6 (see the Supporting Information) in accordance with the NETL reports[8,41] with an annual inflation rate of 3%. In this study, the replacement cost for worn-out equipment is counted in the annual maintenance cost, and the costs of the chemical supplements are calculated from the prices of the chemicals multiplied by the annually required quantities of the corresponding chemicals. The labor cost is estimated from the number of operators per shift multiplied by the base rate of 39.70 $/h (2018$) and 1-year hours with an extra labor burden of 30%.[41]

4. RESULTS AND DISCUSSION

To compare the performance among different CLWS/ITC-CLWS systems and conventional hydrogen production methods using natural gas as the feedstock, Aspen simulations are conducted for cases 0−5 and the ATR process with the same natural gas input (103.2 tons/h at 100% capacity factor). Under this natural gas flow rate, case 0 can achieve a maximum H_2 production of 30 tons/h. The SMR process with CO_2 capture has already been investigated in detail in the NETL baseline report for a given methane feedstock flow rate.[8] Thus, an adjustment in the methane flow rate to match the current flow rate requirement in this study for the SMR case is conducted using a simple feedstock proportional scaling approach to achieve a proper comparison between SMR and other cases.

Considering a desired commercially operational scale CL reactor system, a parallel operational system to process a large amount of the feedstock can be configured as shown in Figure 11, in case one single-reactor configuration is not feasible. For

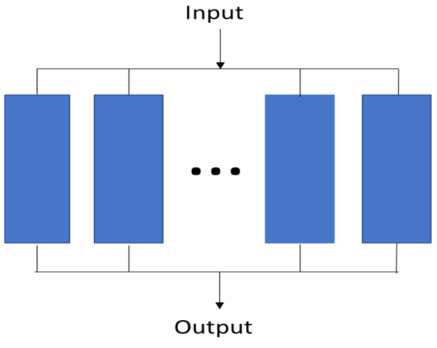


Figure 11. Parallel strategy of the chemical looping reactor system (6 sets of CL reactors in this work).

a hydrogen production of 30 tons/h, a 6-CL reactor assembly system operated in parallel with the same designed capacity of natural gas input for each of the 6 CL reactors is considered. The overall inlet and outlet streams of the 6-CL reactor assembly system are combined and undergo the same upstream and downstream processing. Unlike CLWS/IT-CLWS, it is assumed that the units in the SMR and ATR processes do not have any capacity restraints for the designed natural gas input. Detailed simulation results of OC weight percentages are displayed in Table S7 (see the Supporting Information). In Section 4.1, the reactor designs in cases 0−5 are given and compared, followed by the system performance comparison of electricity and energy conversion in Section 4.2. In Section 4.3, a novel operating strategy to adjust the product structure of electricity and H_2 is introduced and applied to cases 1, 3, 4, and 5. Finally, a detailed economic analysis of cases 0−5 as well as SMR and ATR is given to compare the economic performance.

4.1. Reactor Design. The designed size parameters of the cylindrical reactors and flash drums in the CL system are given in Table 2. In cases 0, 1, and 3, as the inlet and outlet streams

Table 2. CL Reactor and Flash Drum Design

CL case no.		0, 1, 3	2	4	5
reducer	diameter, m	11.89	11.89	4.98	3.93
	height, m	7.13	7.13	2.99	2.36
oxidizer	diameter, m	9.00	8.73	3.25	2.12
	height, m	7.18	7.18	4.50	5.24
combustor	diameter, m	7.49	9.44	5.59	5.64
	height, m	7.49	6.46	4.86	3.99
flash drum (reducer side)	diameter, m	4.67	4.67	2.70	2.50
	height, m	7.00	7.00	6.50	7.40
flash drum (oxidizer side)	diameter, m	3.61	3.50	2.00	1.70
	height, m	5.42	5.25	5.40	5.00

remain unchanged for the CL reactors and flash drums, the reactor sizes are identical. In contrast, case 2 has a smaller amount of steam injection to the oxidizer and a larger air injection to the combustor, which reduce the size of the oxidizer and the flash drum (oxidizer side) but increase the size of the combustor compared to that in case 0.

The reactor sizes of cases 4 and 5 are much smaller than those of low-pressure cases as shown in Table 2. This is because as the pressure increases, the reactor size decreases due to the decrease in the required solid residence time and the increase in the gas density. The density change of steam at elevated pressures also reduces the vapor velocity in the flash drum and causes its diameter to decrease for cases 4 and 5.

4.2. System Performance Comparison. *4.2.1. Electric Power.* The summary of electricity consumption and generation is important for evaluating the energy performance of an industrial system. In this study, the electric power of compressors and turbines is calculated from the Aspen simulation results, while other power-related calculations are scaled from the process equipment as per the NETL baseline reports.[8,9,41]

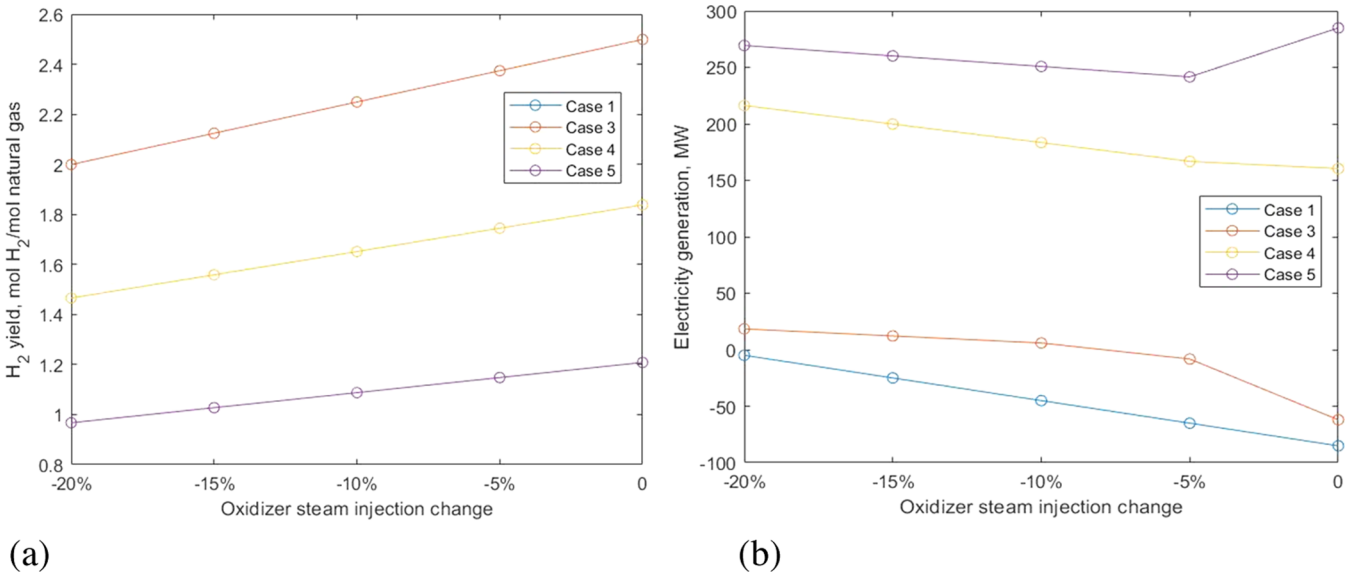
Table S8 (see the Supporting Information) shows the overall electric power summary of cases 0−5, ATR, and SMR. Case 0 consumes the most electricity because of the large compression duty of H_2 and CO_2 as the system operates under a low pressure. By combining the Rankine cycle to utilize the excess heat of the CLWS system, case 1 reduces the electric power demand. In case 2, the integration of the steam turbines with the CLWS system significantly improves the conversion of the thermal energy to electricity, making it a net producer of electric power. Case 3 is an in-between case relative to cases 0 and 2 with the same hydrogen production as case 0 but lesser electric power generation than that of case 2. A huge amount of net electric power is generated for cases 4 and 5 from the steam turbines and the gas turbine due to the large quantities of pressurized hot gas exiting the combustor. Furthermore,

Downloaded from pubs.acs.org/iecred/article-pdf/62/12/5065/1101730/ie2c03834.pdf by DOKUZ EYLUL UNIV user on 01 September 2026

https://doi.org/10.1021/acs.iecr.2c03834
Ind. Eng. Chem. Res. 2023, 62, 5065−5082

Table 3. Overall System Energy Performance at 100% Capacity

case index	0	1	2	3	4	5	ATR	SMR
electricity generation (negative for consumption), MW	−102.2	−85.5	2.5	−62.5	160.0	284.6	−50.0	−33.6
H_2 production, ton/h	30.0	30.0	28.2	30.0	22.1	14.5	25.3	25.3
H_2 yield	2.50	2.50	2.35	2.50	1.84	1.21	2.11	2.10
CGE	0.73	0.73	0.69	0.73	0.54	0.36	0.62	0.62
ETE	0.66	0.67	0.69	0.69	0.66	0.56	0.58	0.59



(a) (b)

Figure 12. (a) Variation of the H_2 yield as the oxidizer steam injection decreases. (b) Variation of electric power generation as the oxidizer steam injection decreases.

significant savings are achieved in the downstream compression duties of CO_2 and H_2 due to a higher operating pressure, resulting in a smaller pressure ratio between that for the final product produced and in the reactor operation. However, as a high-pressure operation demands a higher air inlet flow rate to satisfy the riser gas requirement, more heat is supplied to preheat the air and combustor recycling gas. Therefore, under the autothermal operating conditions, less steam can be generated and injected into the oxidizer for H_2 production. As for the ATR, the ASU unit for oxygen separation consumes the most electricity in contrast to other equipment. The The Rankine cycle which utilizes the combustion heat of recycled fuel gas for power generation does reduce the electricity demand of the system, but the system retains net electric power negative. SMR consumes the least amount of electricity among these cases because it operates at the highest pressure without extra electrical appliances. However, it cannot generate electricity itself because no excess heat is left for utilization in the SMR process.

4.2.2. Overall Energy Performance. Table 3 compares the overall system energy performance of the cases 0−5, ATR, and SMR. The H_2 production calculated in Table 3 represents the pure H_2 mass flow rate with a H_2 volume fraction of over 99.5% in the final product. The purity of H_2 can be further enhanced by simply adding another drying equipment between the H_2 flash drum and the H_2 compressor to remove the small amount of steam in the H_2 product. It should be noted that case 5 generates the most electricity with the least hydrogen production, which is around half of the hydrogen production in case 0. Cases 0, 1, and 3 produce the most hydrogen, i.e., 30 tons/h, while case 2 has a slightly smaller hydrogen production of 28.2 tons/h, followed by the ATR and SMR, which have a production rate of 25.3 tons/h.

As indicated in Table 3, cases 0, 1, 2, and 3 all have promising hydrogen yields of over 2.3. Similar trends are also seen for the CGE. However, when the ETE is used to evaluate both the H_2 production and electric power generation, cases 2 and 3 are the most energy-efficient H_2 production methods with the highest ETE. Case 5, ATR, and SMR have the lowest ETE, which indicates the most energy loss through the exhaust heat and the steam latent heat. It needs to be noted that a typical NGCC plant has an efficiency between 45 and 57%,[53] close to that of case 5, which also has a good amount of electricity generation.

4.3. Novel Operating Strategy. In this section, a novel operating strategy is introduced and evaluated in response to the fluctuating needs for electricity during different time periods. The electrical energy generated has a variety of applications including residential electricity use and industrial use. Because the electric power cannot be stored by itself, the production of electricity highly depends on the demands of customers. This study presents a novel operating strategy to adjust the electricity and H_2 production rate within a certain range.

An assumption is made in this section that a slight change in the steam injection of the CLWS/ITC-CLWS oxidizer does not cause any significant corresponding engineering changes with respect to the equipment or reactor capacity during the operation of the CLWS/ITC-CLWS systems. The strategy is to reduce the steam injection of the oxidizer by no more than 20% and inject more air into the combustor to balance the excess heat generated in cases 1, 3, 4, and 5. Cases 0 and 2 are

https://doi.org/10.1021/acs.iecr.2c03834
Ind. Eng. Chem. Res. 2023, 62, 5065−5082

Downloaded from pubs.acs.org/iecred/article-pdf/62/12/5065/1101730/ie2c03834.pdf by DOKUZ EYLUL UNIV user on 01 September 2026

Table 4. LCOH Comparison of Cases 0−5, ATR, and SMR

case index	0	1	2	3	4	5	ATR	SMR
hydrogen price, $/kg	1.48	1.48	1.42	1.44	1.37	1.78	2.23	1.61

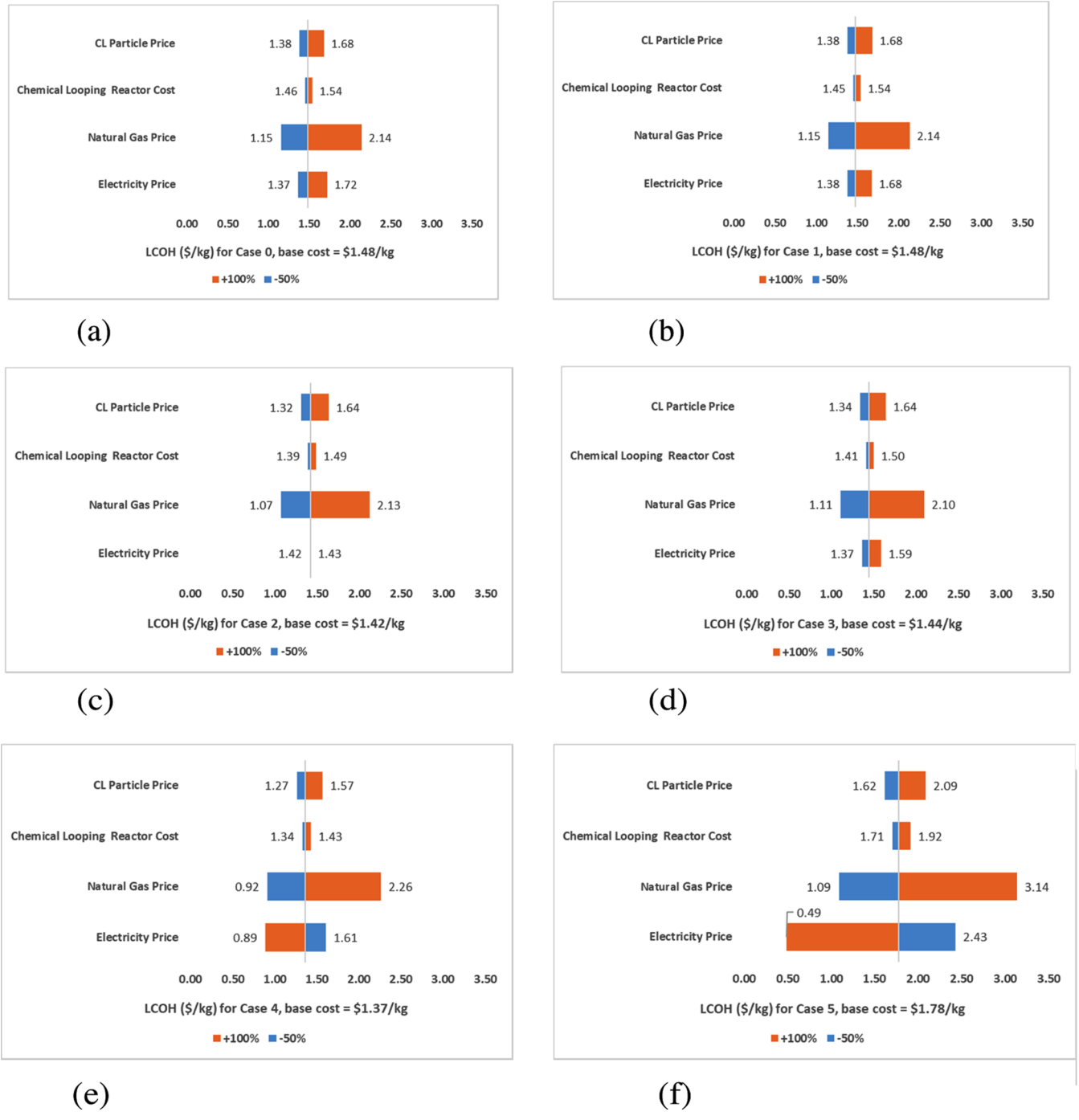


Figure 13. LCOH sensitivity diagrams for CLWS/ITC-CLWS cases 0−5 (a−f).

not considered here because the excess heat in the combustor gas outlet cannot be effectively used without the Rankine cycle. Therefore, the extra heat from the high-pressure exhaust gas can generate more power in the gas turbine for cases 4 and 5. Furthermore, the heat from the exhaust gas coming out of the gas turbine (or the combustor for cases 1 and 3) is also recovered using water/steam and converted into electricity through the steam turbines. It is noted that cases 4 and 5 do not need to recycle the combustor exhaust gas under this strategy. With the new strategy, the overall electric power generation and hydrogen production can be more flexible to satisfy the fluctuating demand of the market.

As shown in Figure 12a, the hydrogen yields of cases 1, 3, 4, and 5 decrease linearly with the reduction percentage of the steam injection. The linear relationship is readily known considering the thermodynamic balance between the gas (H_2/

https://doi.org/10.1021/acs.iecr.2c03834
Ind. Eng. Chem. Res. 2023, 62, 5065−5082

Downloaded from pubs.acs.org/iecred/article-pdf/62/12/5065/1101730/ie2c03834.pdf by DOKUZ EYLUL UNIV user on 01 September 2026

H_2O) and solid ($Fe_{0.947}O/Fe_3O_4$) in the oxidizer. The lines of cases 1 and 3 are overlapped in Figure 12a because of the same injection stream and specification of the CL systems. Compared with cases 4 and 5, cases 1 and 3 clearly have a higher hydrogen yield due to the larger steam injection to the oxidizer. The hydrogen yield of case 5 drops to less than 1 when the steam injection reduces by 20%, which indicates that more chemical energy from the feedstock is transferred to electric power generation instead of hydrogen production.

Figure 12b shows the relationship between the electricity generation and the reduction percentage of the oxidizer steam injection in the CLWS/ITC-CLWS systems. Cases 4 and 5 produce more electricity than that of cases 1 and 3 at the cost of reduction in the hydrogen yield. Cases 1 and 4 both exhibit a nearly linear relationship between the two parameters, while cases 3 and 5 show some different behaviors from 0 to −5% change of the oxidizer steam injection. For case 3, the 5% reduction in the steam injection causes more water to go through the steam turbine instead of direct heating before entering the oxidizer, thus resulting in a sharp increase in electricity generation. For case 5, the removal of combustor exhaust gas recycling results in a higher raw air injection to the combustor. The larger air flow rate demands considerably more compression duty from the air compressor. Consequently, the huge consumption of electricity leads to a decrease in the net electric power generation. Overall, the new operating strategy yields attractive outcomes for cases 1, 3, and 4, resulting from the adjustment of the hydrogen and electricity production structure based on the analysis given above.

4.4. Economic Performance Analysis. *4.4.1. Economic Assessment and Comparison.* Table S9 (see the Supporting Information) shows the itemized costs of the capital costs, the O&M costs, and the fuel costs for cases 0−5, ATR, and SMR. Table S9 (see the Supporting Information) reveals that the low-pressure CLWS/ITC-CLWS cases require much less capital investment compared to ATR and SMR that require expensive MDEA/MEA CO_2 removal systems. The high-pressure ITC-CLWS cases have a higher TPC than that of the low-pressure cases because of the expensive turbine, air compressor, and heat recovery system. The capital cost of the ATR process is the highest due to the use of the expensive ASU. Operating labor is estimated based on the major equipment number with reference to the NETL reports,[8,41] and the rest of the fixed O&M costs are calculated proportionally to the labor cost or the total plant cost as per Table S4 (see the Supporting Information). The natural gas cost remains unchanged in all cases because of the same natural gas feedstock flow rate. The variable O&M costs have the greatest impact on the hydrogen production cost over the 30-year operating period. Among the eight cases, cases 2, 4, and 5 have the lowest variable O&M expenses because no electricity purchase is required for these cases. However, it needs to be noted that the CO_2 capture percentage of SMR and ATR can only reach around 90%, compared to the 100% CO_2 capture in the CLWS/ITC-CLWS cases. Thus, an extra CO_2 emission tax is added for the ATR and SMR cases.

Although SMR is a cost-effective H_2 production method industrially,[54] the CLWS/ITC-CLWS methods can produce H_2 at lower costs based on economic assessment analysis. As Table 4 indicates, case 4 achieves the lowest LCOH of $1.37/kg and ATR comes out to be the most expensive method with the highest LCOH of $2.23/kg. 15% cost reduction can be achieved by replacing SMR with the ITC-CLWS method of case 4. The impact of the capital factor on the LCOH is not significant, which is indicated in Table S10 (see the Supporting Information).

4.4.2. Economic Sensitivity Analysis. In this section, an economic sensitivity analysis is conducted to examine the influence of the CL particle price, the CL reactor cost, the natural gas price, and the electricity price on the LCOH for cases 0−5. The LCOH is calculated and presented as the parameter over the range from −50 to +100% of its base value.

The natural gas price is the most dominant factor and has the greatest influence on the LCOH as indicated in Figure 13. Compared with other factors, the CL reactor cost has the least effect on the LCOH. The electricity price also has a considerable influence on the LCOHs of cases 4 and 5 where significant quantities of net electricity generation exist. Case 2 is almost electricity-neutral, so the electricity price has a negligible effect on its LCOH. Compared with low-pressure cases, the LCOHs of cases 4 and 5 are more susceptible to electricity and natural gas price fluctuations due to the large amount of electricity generation and less hydrogen production. It is noted that the LCOH of case 5 is $0.49/kg when the electricity price is doubled, which indicates that the electric power income can cover most of the production cost in case 5. The CL particle cost has a moderate effect on the LCOH, and the variation of this factor results in about 7−18% change of the LCOHs in six cases.

5. CONCLUSIONS

In this study, novel ITC-CLWS process schemes for hydrogen production coupled with electricity cogeneration are conceived by integrating steam turbines into the standard CLWS process configuration to enhance the thermal efficiency. The ITC-CLWS processes under different pressures in operation are considered and simulated using ASPEN for their process conversion efficiencies. In addition to the thermodynamic simulation, this study also accounts for the desired riser gas flow that lifts the particles through the riser in a circulatory motion from the combustor to the reducer. The simulation results indicate that the new ITC-CLWS systems under atmospheric pressure (cases 2 and 3) can achieve a higher ETE (69%) compared to those from the conventional H_2 production processes represented by the ATR (58%) and SMR (59%). The standard CLWS systems and ITC-CLWS systems can both also achieve a CGE as high as 73%, while the CGE of the ATR and SMR can only reach 62%. Furthermore, a novel operating strategy is presented that can adjust the electricity and hydrogen production ratio to meet the fluctuating market demand. The new operating strategy has proved to be effective for CLWS/ITC-CLWS systems under 1 bar and 10 bar.

A detailed economic assessment is also conducted for the processes of CLWS, ITC-CLWS, ATR, and SMR. The itemized costs of equipment and reactors are assessed from the scaling approach based on those of the reference process units given in the NETL baseline reports. The results indicate that the CLWS/ITC-CLWS systems require less capital cost compared to the ATR and SMR systems, while the operating costs vary in comparison depending on the net electric power demand. The LCOHs of CLWS/ITC-CLWS systems are calculated and compared to those of the ATR and SMR. Among all the cases considered, the high-pressure ITC-CLWS scheme (10 bar, case 4) can achieve the lowest LCOH of $1.37/kg, while the ATR yields the largest LCOH of $2.23/kg.

Downloaded from pubs.acs.org/iecred/article-pdf/62/12/5065/1101730/ie2c03834.pdf by DOKUZ EYLUL UNIV user on 01 September 2026

https://doi.org/10.1021/acs.iecr.2c03834
Ind. Eng. Chem. Res. 2023, 62, 5065−5082

Moreover, an economic sensitivity analysis of the costs of the CL particle, CL reactor, natural gas, and electricity was conducted for the CLWS/ITC-CLWS cases. The result indicates that the natural gas cost has the largest effect on the LCOH, while the CL reactor cost has the smallest effect. Overall, the ITC-CLWS system can achieve a higher energy efficiency and a better economic outcome compared to the standard CLWS system with a moving bed reducer and ATR and SMR processes for H_2 production.

■ ASSOCIATED CONTENT

Supporting Information

The Supporting Information is available free of charge at https://pubs.acs.org/doi/10.1021/acs.iecr.2c03834.

SMR with CO_2 capture; simulation model setup; natural gas composition; additional assumptions used in the process analysis; cost estimation methodology; scale function parameters for the main equipment; general assumptions of prices regarding O&M costs and fuel costs; OC weight percentage among the chemical looping reactors; electricity consumption and generation for different cases at 100% load; overall itemized cost assessment; and LCOH calculated with different capital factors for all equipment (except chemical looping reactors and flash drum) (PDF)

■ AUTHOR INFORMATION

Corresponding Author

Liang-Shih Fan − *William G. Lowrie Department of Chemical and Biomolecular Engineering, Columbus, Ohio 43210, United States;* orcid.org/0000-0002-3892-5362; Email: fan.1@osu.edu

Authors

Qiaochu Zhang − *William G. Lowrie Department of Chemical and Biomolecular Engineering, Columbus, Ohio 43210, United States;* orcid.org/0000-0002-3630-8125

Andrew Tong − *William G. Lowrie Department of Chemical and Biomolecular Engineering, Columbus, Ohio 43210, United States;* orcid.org/0000-0002-4281-1317

Complete contact information is available at: https://pubs.acs.org/10.1021/acs.iecr.2c03834

Author Contributions

Q.Z.: conceptualization, methodology, software, formal analysis, and writing—original draft. A.T.: supervision. L.-S.F.: conceptualization, supervision, and writing—review and editing.

Funding

The C. John Easton Professorship Endowment was used to support this research.

Notes

The authors declare no competing financial interest.

■ ACKNOWLEDGMENTS

The authors would like to thank Anuj Joshi and Pinak Mohapatra for their assistance in the preparation of the article and Dikai Xu and Dawei Wang for the constructive discussion on the reactor design considered in this study.

■ ABBREVIATIONS

ASME	American Society of Mechanical Engineers
ATR	autothermal reforming
ASU	air separation unit
ATWACC	after-tax weighted average cost of capital
BEC	bare erected cost
CEPCI	chemical engineering plant cost index
CF	capacity factor
CGE	cold gas efficiency
CL	chemical looping
CLC	chemical looping combustion
CLPO	chemical looping partial oxidation
CLWS	chemical looping water splitting
EIA	Energy Information Administration
ECHF	Eng'g CM, H.O. & Fee, engineering, construction management, home office & fees
ETE	effective thermal efficiency
FC	financing costs
HP	high pressure
IC	inventory capital
ICC	inventory capital costs
ICCC	initial costs for catalyst and chemicals
IP	intermediate pressure
ITC-CLWS	integrated turbine-combined chemical looping water splitting
IU	international units
LCOH	levelized cost of hydrogen
LHV	lower heating value
LP	low pressure
MFV	superficial gas velocity at minimum fluidization
MM	maintenance material
NETL	National Energy Technology Laboratory
NGCC	natural gas combined cycle
OC	oxygen carrier
OOC	other owner's costs
OSU	Ohio State University
O&M	operation and maintenance
PC	preproduction costs
PSA	pressure swing adsorption
SMR	steam methane reforming
TBC	to be calculated
TOC	total overnight costs
TPC	total plant cost
WGS	water−gas shift

■ REFERENCES

(1) International Energy Agency. *The Future of Hydrogen: Seizing Today's Opportunities*; IEA Publication, 2019; p 203.

(2) Christensen, A. *Assessment of Hydrogen Production Costs from Electrolysis: United States and Europe*; International Council on Clean Transportation, 2020.

(3) Department of Energy. Hydrogen Production Processes. https://www.energy.gov/eere/fuelcells/hydrogen-production-processes (accessed August 12, 2022).

(4) Liu, K.; Song, C.; Subramani, V. *Hydrogen and Syngas Production and Purification Technologies*; John Wiley & Sons, 2009; pp 1−533.

(5) U.S. Department of Energy. *Hydrogen Strategy: Enabling A Low-Carbon Economy*; Department of Energy: Washington, DC, USA, 2020.

(6) Das, H. S.; Chowdhury, M. F. F.; Li, S.; Tan, C. W. Fuel Cell and Hydrogen Power Plants. In *Hybrid Renewable Energy Systems and Microgrids*; Elsevier, 2021; pp 313−349.

(7) Khojasteh Salkuyeh, Y.; Saville, B. A.; MacLean, H. L. Techno-Economic Analysis and Life Cycle Assessment of Hydrogen

Downloaded from pubs.acs.org/iecred/article-pdf/62/12/5065/1101730/ie2c03834.pdf by DOKUZ EYLUL UNIV user on 01 September 2026

Production from Natural Gas Using Current and Emerging Technologies. *Int. J. Hydrogen Energy* **2017**, *42*, 18894−18909.
(8) Rath, L. K.; Chou, V. H.; Kuehn, N. J. *Assessment of Hydrogen Production with CO2 Capture Volume 1: Baseline State-of-the-Art Plants*; National Energy Technology Laboratory: Pittsburgh, PA, United States, 2011.
(9) Summers, W. *Baseline Analysis of Crude Methanol Production from Coal and Natural Gas*; National Energy Technology Laboratory, 2014; pp 1−83.
(10) Lavoie, J. M. Review on Dry Reforming of Methane, a Potentially More Environmentally-Friendly Approach to the Increasing Natural Gas Exploitation. *Front. Chem.* **2014**, *2*, No. 81.
(11) Voitic, G.; Pichler, B.; Basile, A.; Iulianelli, A.; Malli, K.; Bock, S.; Hacker, V. *Hydrogen Production*; Hacker, V.; Mitsushima, S. B., Eds.; Elsevier, 2018; Chapter 10, pp 215−241. DOI: 10.1016/B978-0-12-811459-9.00010-4.
(12) Basile, A.; Liguori, S.; Iulianelli, A. Membrane Reactors for Methane Steam Reforming (MSR). In *Woodhead Publishing Series in Energy*; Basile, A.; Di Paola, L.; Hai, F.; Piemonte, V. B., Eds.; Woodhead Publishing, 2015; Chapter 2, pp 31−59. DOI: 10.1016/B978-1-78242-223-5.00002-9.
(13) Muradov, N. Low to Near-Zero CO2 Production of Hydrogen from Fossil Fuels: Status and Perspectives. *Int. J. Hydrogen Energy* **2017**, *42*, 14058−14088.
(14) Fan, L.-S. *Chemical Looping Systems for Fossil Energy Conversions*; John Wiley & Sons, 2011.
(15) Fan, L.-S. *Chemical Looping Partial Oxidation: Gasification, Reforming, and Chemical Syntheses*; Cambridge University Press, 2017.
(16) Zhang, Y.; Wang, D.; Pottimurthy, Y.; Kong, F.; Hsieh, T.-L.; Sakadjian, B.; Chung, C.; Park, C.; Xu, D.; Bao, J.; Velazquez-Vargas, L.; Guo, M.; Sandvik, P.; Nadgouda, S.; Flynn, T. J.; Tong, A.; Fan, L.-S. Coal Direct Chemical Looping Process: 250 KW Pilot-Scale Testing for Power Generation and Carbon Capture. *Appl. Energy* **2021**, *282*, No. 116065.
(17) Lyngfelt, A.; Brink, A.; Langørgen, Ø.; Mattisson, T.; Rydén, M.; Linderholm, C. 11,000 h of Chemical-Looping Combustion Operation—Where Are We and Where Do We Want to Go. *Int. J. Greenhouse Gas Control* **2019**, *88*, 38−56.
(18) Mei, D.; Linderholm, C.; Lyngfelt, A. Performance of an Oxy-Polishing Step in the 100 KW Th Chemical Looping Combustion Prototype. *Chem. Eng. J.* **2021**, *409*, No. 128202.
(19) Zhang, Y.; Kong, F.; Tong, A.; Fan, L. S. Autothermal Operation Strategies of Chemical Looping Processes for Hydrogen Generation: Process Simulation, Parametric Studies, and Exergy Analysis. *Ind. Eng. Chem. Res.* **2020**, *59*, 5877−5890.
(20) Liu, Y.; Qin, L.; Cheng, Z.; Goetze, J. W.; et al. Near 100% CO Selectivity in Nanoscaled Iron-Based Oxygen Carriers for Chemical Looping Methane Partial Oxidation. *Nat. Commun.* **2019**, *10*, No. 5503.
(21) Kong, F.; Zhang, Q.; Liu, Y.; Swift, J.; Tene Youmbi, D.; Tong, A.; Fan, L.-S. Process Analysis of Chemical Looping Systems for Dimethyl Ether Synthesis from Coal. *Trans. Indian Natl. Acad. Eng.* **2020**, *5*, 17−26.
(22) Hsieh, T. L.; Xu, D.; Zhang, Y.; Nadgouda, S.; Wang, D.; Chung, C.; Pottimurphy, Y.; Guo, M.; Chen, Y. Y.; Xu, M.; He, P.; Fan, L. S.; Tong, A. 250 kWth High Pressure Pilot Demonstration of the Syngas Chemical Looping System for High Purity H2 Production with CO2 Capture. *Appl. Energy* **2018**, *230*, 1660−1672.
(23) Kong, F.; Swift, J.; Zhang, Q.; Fan, L. S.; Tong, A. Biogas to H2 Conversion with CO2 Capture Using Chemical Looping Technology: Process Simulation and Comparison to Conventional Reforming Processes. *Fuel* **2020**, *279*, No. 118479.
(24) He, F.; Huang, Z.; Wei, G.; Zhao, K.; Wang, G.; Kong, X.; Feng, Y.; Tan, H.; Hou, S.; Lv, Y.; Jiang, G.; Guo, Y. Biomass Chemical-Looping Gasification Coupled with Water/CO2-Splitting Using NiFe2O4 as an Oxygen Carrier. *Energy Convers. Manage.* **2019**, *201*, No. 112157.
(25) Chiesa, P.; Lozza, G.; Malandrino, A.; Romano, M.; Piccolo, V. Three-Reactors Chemical Looping Process for Hydrogen Production. *Int. J. Hydrogen Energy* **2008**, *33*, 2233−2245.
(26) He, Y.; Zhu, L.; Li, L.; Liu, G. Hydrogen and Power Cogeneration Based on Chemical Looping Combustion: Is It Capable of Reducing Carbon Emissions and the Cost of Production. *Energy Fuels* **2020**, *34*, 3501−3512.
(27) Cormos, C. C.; Cormos, A. M.; Petrescu, L. Assessment of Chemical Looping-Based Conceptual Designs for High Efficient Hydrogen and Power Co-Generation Applied to Gasification Processes. *Chem. Eng. Res. Des.* **2014**, *92*, 741−751.
(28) Cormos, C. C. Hydrogen Production from Fossil Fuels with Carbon Capture and Storage Based on Chemical Looping Systems. *Int. J. Hydrogen Energy* **2011**, *36*, 5960−5971.
(29) Vundela Siva, R.; Subash Chndra, K.; Sudhir Kumar, T.; Narayanlal, P. An Approach to Analyse Energy and Exergy Analysis of Thermal Power Plants: A Review. *Smart Grid Renewable Energy* **2010**, *1*, 143−152.
(30) Zoelle, A.; Keairns, D.; Pinkerton, L. L.; Turner, M. J.; Woods, M.; Kuehn, N.; Shah, V.; Chou, V. *Cost and Performance Baseline for Fossil Energy Plants Volume 1a: Bituminous Coal (PC) and Natural Gas to Electricity Revision 3*; National Energy Technology Laboratory (NETL): Pittsburgh, PA, Morgantown, WV, United States, 2015.
(31) Suppes, G. J.; Storvick, T. S. Production of Electricity. In *Sustainable World Sustainable Nuclear Power*; Academic Press: Cambridge, MA, USA, 2007.
(32) Kathe, M. V.; Empfield, A.; Na, J.; Blair, E.; Fan, L. S. Hydrogen Production from Natural Gas Using an Iron-Based Chemical Looping Technology: Thermodynamic Simulations and Process System Analysis. *Appl. Energy* **2016**, *165*, 183−201.
(33) Pattipati, R. R.; Wen, C. Y. Minimum Fluidization Velocity at High Temperatures. *Ind. Eng. Chem. Process Des. Dev.* **1981**, *20*, 705−707.
(34) Mendiara, T.; Abad, A.; de Diego, L. F.; García-Labiano, F.; Gayán, P.; Adánez, J. Reduction and Oxidation Kinetics of Tierga Iron Ore for Chemical Looping Combustion with Diverse Fuels. *Chem. Eng. J.* **2019**, *359*, 37−46.
(35) Fogler, H. S. Diffusion and Reaction. In *Elements of Chemical Reaction Engineering*; Pearson Education Limited; Chapter 12, 2016.
(36) Cai, P.; Michele, G. D.; Gradassl, A. T. A Generalized Method for Predicting Gas Flow Distribution between the Phases in FBC. In *Fluidized Bed Combustion*; J-GLOBAL, 1993; Vol. 2, pp 991−1002.
(37) Fan, L. S.; Zhu, C. *Principles of Gas-Solid Flows*; Cambridge University Press: Port Chester, NY, United States, 1999.
(38) Keyes, D. B.; Soukup, R.; Nichols, W. A. Design of Fractionating Columns. *Ind. Eng. Chem.* **1928**, *20*, 464−466.
(39) Kong, F.; Li, C.; Zhang, Y.; Gu, Y.; Kathe, M.; Fan, L. S.; Tong, A. Hydrogen Production from Natural Gas Using an Iron-Based Chemical Looping Technology: Process Modeling, Heat Integration, and Exergy Analysis. *Energy Technol.* **2020**, *8*, No. 1900377.
(40) Zeng, L.; He, F.; Li, F.; Fan, L. S. Coal-Direct Chemical Looping Gasification for Hydrogen Production: Reactor Modeling and Process Simulation. *Energy Fuels* **2012**, *26*, 3680−3690.
(41) Fout, T.; Zoelle, A.; Keairns, D.; Turner, M.; Woods, M.; Kuehn, N.; Shah, V.; Chou, V.; Pinkerton, L. *Cost and Performance Baseline for Fossil Energy Plants Volume 1a: Bituminous Coal (PC) and Natural Gas to Electricity Revision 3*; National Energy Technology Laboratory: Pittsburgh, PA, United States, 2015; Vol. *1*, p 240.
(42) Branker, K.; Pathak, M. J. M.; Pearce, J. M. A Review of Solar Photovoltaic Levelized Cost of Electricity. *Renewable Sustainable Energy Rev.* **2011**, *15*, 4470−4482.
(43) Wimer, J. G.; Summers, W. M. *Quality Guideline for Energy System Studies: Cost Estimation Methodology for NETL Assessments of Power Plant Performance*; National Energy Technology Laboratory: Pittsburgh, PA, United States, 2011.
(44) Theis, J. *Quality Guidelines for Energy Systems Studies: Cost Estimation Methodology for NETL Assessments of Power Plant Performance*; National Energy Technology Laboratory: Pittsburgh, PA, United States, 2021.

Downloaded from pubs.acs.org/iecred/article-pdf/62/12/5065/1101730/2/ie2c03834.pdf by DOKUZ EYLUL UNIV user on 01 September 2026

(45) Mignard, D. Correlating the Chemical Engineering Plant Cost Index with Macro-Economic Indicators. *Chem. Eng. Res. Des.* **2014**, *92*, 285−294.
(46) Clayton, T.; Baumann, P. E.; et al. Cost-to-Capacity Method: Applications and Considerations. *M&TS J.* **2014**, *30*, 49−56.
(47) Keairns, D.; Kuehn, N.; Newby, R.; Shah, V. *Guidance for NETL's Oxycombustion R&D Program: Chemical Looping Combustion Reference Plant Designs and Sensitivity Studies*; National Energy Technology Laboratory (NETL): Pittsburgh, PA, United States, 2014.
(48) Pastor, T. P.; Vattappilly, J. Section VIII−Division I: Rules for Construction of Pressure Vessels. In *Online Companion Guide to the ASME Boiler and Pressure Vessel Codes: Criteria and Commentary on Select Aspects of the Boiler & Pressure Vessel Codes*; ASME Press, 2020.
(49) Nelson, D. A.; Kirkwood, R. L.; Douglas, J. M. Conceptual Design of Chemical Processes. *Simul. Ser.* **1989**, *20*, 180−184.
(50) US Energy Information Administration. *Annual Energy Outlook 2022*, DOE/EIA-0035(2022/7); US Energy Information Administration, 2022.
(51) United States Natural Gas Industrial Price (Dollars per Thousand Cubic Feet). https://www.eia.gov/dnav/ng/hist/n3035us3a.htm (accessed August 12, 2022).
(52) Smith, E.; Morris, J.; Kheshgi, H.; Teletzke, G.; Herzog, H.; Paltsev, S. The Cost of CO2 Transport and Storage in Global Integrated Assessment Modeling. *Int. J. Greenhouse Gas Control* **2021**, *109*, 1−76.
(53) Storm, K. Combined Cycle Power Plant (1× 1) Labor Estimate. In *Industrial Construction Estimating Manual*; Gulf Professional Publishing, 2020; pp 95−159.
(54) Basile, A.; Liguori, S.; Iulianelli, A. *Membrane Reactors for Methane Steam Reforming (MSR)*; Elsevier Ltd, 2015. DOI: 10.1016/B978-1-78242-223-5.00002-9.

Downloaded from pubs.acs.org/iecred/article-pdf/62/12/5065/1101730 2/ie2c03834.pdf by DOKUZ EYLUL UNIV user on 01 September 2026

https://doi.org/10.1021/acs.iecr.2c03834
Ind. Eng. Chem. Res. 2023, 62, 5065−5082